

UNIVERSITY OF CINCINNATI

Date: _____

I, _____,
hereby submit this work as part of the requirements for the degree of:

in:

It is entitled:

This work and its defense approved by:

Chair: _____

Development of a Data Acquisition System and Piezoelectric Sensors for an Experimental Structural Neural System

Thesis submitted to the faculty of the University of Cincinnati in partial fulfillment of the
requirements for the degree of

Masters of Science

in

Mechanical Engineering

Dr. Mark Schulz, Advisor

Dr. David Thompson Co-Advisor

Dr. Vesselin Shanov

June 7, 2005

Cincinnati, Ohio

Abstract

This thesis develops a data acquisition system and long piezoelectric sensors for a technique of structural health monitoring based on a structural neural system and continuous sensors. The structural neural system uses distributed sensing and parallel signal processing in real time to monitor large structures like an aircraft for damage. The structural neural system consists of piezoceramic nerves and electronic logic circuits and was tested on an aluminum plate that was fatigue loaded using a mechanical testing machine. The testing indicated that the SNS analog processor using conventional monolithic piezoceramic sensors was able to detect the acoustic emissions using continuous fiber sensors. The acoustic emission level in aluminum was small but detectable. A higher sensitivity of the neural system was needed. Therefore, further sensor development was undertaken including fabricating piezoelectric active fiber continuous sensors. The testing in this thesis indicates that the continuous sensor can be closer to the damage site, and is more sensitive than conventional discrete sensors. In this thesis a data acquisition system was developed using LabVIEW and single fiber continuous sensors were developed for the structural neural system. The testing indicates that the structural neural system will be able to continuously monitor a structure and provide a long-term history of the health of the structure.

Acknowledgement

The work for this thesis was carried out in the Smart Structures and Bio-Nanotechnology Lab of the Department of Mechanical Engineering at University of Cincinnati.

The supervisor of the work was Dr. Mark Schulz. I am grateful for his invaluable support. I also want to thank the committee members, Dr. David Thompson and Shannov Vesselin. I have worked for 2 years in the group of Dr Schulz, who has not only given me excellent guidance but also helped in meeting the innovative and challenging requirements of my thesis

Team work made the topic of the thesis both "magnetic" and "stimulating". Goutham Kirikera deserves my warmest thanks for many discussions and friendship. I want to thank my lab-members YeoHeung Yun, Atul Miskin, Sourabh Datta and Ramanand. I wish to express my gratitude to Prasad Kadam for reviewing the manuscript of this thesis.

I am very grateful for the love and support of my parents and my roommates, Nitin and Prasad.

ABSTRACT.....	III
CHAPTER 1 INTRODUCTION.....	1
1.1 Structural Health Monitoring.....	1
1.1.1 Active structural health monitoring	1
1.1.2 Passive structural health monitoring.....	1
1.2 Piezoceramic Material	4
1.3 Interdigitated Electrode Monolithic Ceramics	5
1.4 Piezoelectric Active fiber composite.....	6
1.5 The Macro fiber composite	7
1.6 Continuous Sensors.....	8
1.7 Objective of the Research.....	9
CHAPTER 2 ACTIVE FIBER COMPOSITES	11
2.1 Modeling Active Fiber Composite Sensors.....	12
2.2 Design of Active Fiber Composites.....	15
2.3 Fiber Material	15
2.4 Fiber cross section.....	17
2.5 Composite thickness.....	18
2.6 Matrix Material.....	18
2.7 Electroding.....	19
2.8 Summary.....	21
CHAPTER 3 MANUFACTURING OF ACTIVE FIBER SENSORS	22
3.1 Mold	24
3.2 Manufacturing process.....	27
3.2.1 Casting	27

3.2.2	Curing	30
3.2.3	Electroding.....	30
3.2.4	Field Installation Procedure	33
3.2.5	Poling	37
CHAPTER 4 THE DATA ACQUISITION SYSTEM.....		41
4.1	Hardware Design	42
4.1.1	Signal Type	42
4.1.2	Voltage range	43
4.1.3	Resolution	43
4.1.4	Number of Input channels.....	43
4.1.5	Simultaneous sampling	43
4.1.6	Sampling rate	44
4.2	Software Design.....	45
4.2.1	Prior Work	45
4.2.2	Limitations of Prior Solutions.....	46
4.2.3	Problem Statement	46
4.2.4	Specifications.....	46
4.2.5	Development of the LabVIEW system.....	50
4.3	Testing and Debugging	52
4.3.1	Finding Errors	53
4.3.2	Execution Highlighting.....	53
4.3.3	Single-Stepping.....	53
4.3.4	Probes.....	53
4.3.5	Breakpoints	53
CHAPTER 5 EXPERIMENTATION		56
5.1	Testing the SNS on a Riveted Aluminum Plate using Lead Breaks.....	56
5.2	Capacitance effect of the sensor.....	59
5.3	Pulse Excitation.....	61
5.4	Dynamic Testing of an aluminum plate	63
5.5	Fatigue Testing of a Riveted Aluminum Joint	63
5.6	Monitoring AE on an Aluminum Plate using the SNS	66
CHAPTER 6 SENSOR CHARACTERIZATION		69
6.1	Low frequency response of the sensor	70

6.2	High frequency response of the sensor (Lead Break).....	73
6.3	High frequency response of the sensors in a series connection (Lead Break).....	76
6.4	High frequency response of the sensors for a parallel connection (Lead Break).....	78
6.5	AFC actuation	80
6.6	Power Harvesting.....	82
6.7	Calculating the d_{31} coefficient	84
CHAPTER 7 CONCLUSION		87
CHAPTER 8 FUTURE WORK		88
8.1	Data acquisition system	88
8.2	Active Fiber Sensor	89
REFERENCES.....		90
APPENDIX A		99
LabVIEW Code Description		99
APPENDIX B		103
Matlab® Script		103
APPENDIX C		105
PCI 6110E Board Specifications.....		105
APPENDIX D		109
Specification of Silver conductive epoxy		109

Table of Figures

Figure 1.1 Monolithic PZT patch [9]	5
Figure 1.2 Interdigital Electrode Monolithic Ceramic [15]	6
Figure 1.3 Piezoelectric Active Fiber Composites [9]	7
Figure 1.4 Components of Macro Fiber Composites [K. Wilikie, 14]	8
Figure 2.1 Flowchart of Active Fiber Sensor Design	15
Figure 2.2 Types of PZT fibers	17
Figure 3.1 Void formation in AFC preform	23
Figure 3.2 AFC casting Mold	25
Figure 3.3 Injector Assembly	26
Figure 3.4 PZT fiber size $165.1mm \times 0.75mm \times 0.25mm$ [23]	28
Figure 3.5 Curing for the AFC Sensor	30
Figure 3.6 Structure Integrated electroding	32

Figure 3.7 Stand-alone Electroding	32
Figure 3.8 Sensor field installation procedure	34
Figure 3.9 Weiss domains; (a) Before poling; (b) During Poling; (c) After Poling	37
Figure 3.10 Poling setup (a) Poling fixture (b) Entire Poling Setup	39
Figure 3.11 Poling Wiring Diagram	39
Figure 3.12 Manufactured Active Fiber Composite Sensor	40
Figure 4.1 Data Acquisition System	41
Figure 4.2 Software Requirements	47
Figure 4.3 Sensing architecture	52
Figure 4.4 LabVIEW front panel layout a) Trigger parameters; (b) analysis parameters (c) date and total running time and number of stress cycles; (d) firing neurons and LP filtered cumulative AE voltage; (e) displayed parameter depending on the tab control; (f) LED indicator showing AE; (g) number of stress cycles; (h) frequency of vibration (i) Stop button to stop execution of the Virtual Instrument; (j) Loading frequency	55

Figure 5.1 Aluminum Rivet Plate; (a) Picture of the plate, (b) Geometric model of the riveted plate along with sensors	57
Figure 5.2 Response of SNS for an AE lead break located near Sensor 4; (a) Crack information, (b) Time waveform of the cumulative AE	58
Figure 5.3 Response of SNS for an AE lead break located near sensor 2; a) Crack	58
Figure 5.4 Measurement of Impedance of the Kapton [®] and superglue layer (a) Impedance measurement circuit, (b) Variation of Impedance with frequency	61
Figure 5.5 Excitation to the PZT; (a) Pulse Excitation, (b) Response of sensors 2, 3 and 4 for a pulse excitation to PZT-1	62
Figure 5.6 Actuation through the joint; (a) Response of sensors 2 and 4 for an excitation with PZT 3; (b) Response of sensors 2, 3 and 4 for a pulse excitation from PZT-5	63
Figure 5.7 Setup of MTS machine and LabVIEW data acquisition system to test the riveted aluminum plate	64
Figure 5.8 Response of SNS for an AE lead break located near sensor 4, (a) Crack Information, and (b) Time waveform of AE	65

Figure 5.9 Response of SNS for an AE lead break located near sensor 2, a) Crack Information b) Time waveform of AE	65
Figure 5.10 Geometry of a narrow aluminum plate with supports	66
Figure 5.11 Crack generated due to loading the aluminum plate on the MTS machine (the plate is straight and finally fractured without bending)	67
Figure 5.12 Response of SNS analog processor; (a) Crack Location Information, and (b) Time domain waveform	68
Figure 6.1 Fiber glass plate size with three bonded Active fiber composite sensors	69
Figure 6.2 Simply supported beam	70
Figure 6.3 Response of sensor-1, 2, 3 for low frequency tap at sensor-1	71
Figure 6.4 Response of sensor-1, 2,3 for low frequency tap at sensor-2	71
Figure 6.5 Response of sensor-1, 2,3 for low frequency tap at sensor-3	72
Figure 6.6. Lead break location on the beam plate	73
Figure 6.7 Lead break response for sensor-1	74
Figure 6.8 Lead break response for sensor-2	74

Figure 6.9 Lead break response for sensor-3	75
Figure 6.10 Lead break response for sensor-2 (a) and frequency response for sensor-2 (b)	75
Figure 6.11 Response for Sensors in Series, lead break location near sensor-1	76
Figure 6.12 Response for Sensors in Series, lead break location near sensor-2	77
Figure 6.13 Response for Sensors in Series, lead break location near sensor-3	77
Figure 6.14 Response for Sensors in parallel, lead break location near sensor-1	78
Figure 6.15 Response for Sensors in parallel, lead break location near sensor-2	79
Figure 6.16 Response for Sensors in parallel, lead break location near sensor-3	79
Figure 6.17 Response of Sensors-1 and 3 for actuation at AFC-2	81
Figure 6.18 Response of Sensors-1 and 3 for actuating sensor-2	81
Figure 6.19 Experimental setup for power harvesting of sensors bonded on the beam	82
Figure 6.20 Response from sensor-2 under sinusoidal MTS loading	83
Figure 6.21 A composite beam under loading	84

List of tables

Table 1.1 Behavior of various Active Materials

Table 2.1 Comparison of one-dimensional properties of PZT ceramics [4-6]

Table 2.2 Typical Properties of the conductive epoxy H20E (Epoxy Technology, Inc.)

Table 3.1 Manufacturing Tolerance for the AFC preform

Table 3.2 Steps in PZT poling

Table 3.3 AFC sensor dimensions

Table 4.1 Comparison of various software design environment

Table 4.2 Sub VI in shm.vi

Table 4.3 Number of channels

Table 5.1 Pre-Assigned Voltages for Different Neurons.

Table 6.1 Values used in equation 6.9.

Table 6.2 Comparison of Results

Chapter 1 Introduction

In the current economic climate it is desirable that the life of a given structure like an aircraft or bridge be as long as possible. These structures must remain in operation for longer periods of time. However this expectation or rather the economic need has driven the field of structural health monitoring. Structural Health Monitoring (SHM) involves implementing damage detection and monitoring strategies to extend the life of engineering infrastructure. Structural health monitoring helps in making decisions regarding the use, maintenance and retirement of structures under monitoring.

1.1 Structural Health Monitoring

SHM can be considered as the identification of signals which are caused or modified by damage in a structure. SHM can be broadly divided into two types; namely active structural health monitoring and passive structural health monitoring, which are discussed below.

1.1.1 Active structural health monitoring

Active SHM requires the use of both sensors and actuators. Thereby, the location and magnitude of the damage are determined due to wave propagation processes. These methods need external power for health monitoring [1].

1.1.2 Passive structural health monitoring

Passive SHM techniques don't use external power for structural health monitoring. This method is termed passive because the operator waits for an internal dislocation in response to a change in loading, and solves for the damage source kinematics. They use

properties such as change in resistance, change in strain, or sensing Acoustic Emissions (AE). Various passive techniques are available for SHM like fiber optic strain measurement, etc. [2]. The AE technique is a fast, accurate cost effective method [3] that is applied for monitoring the health of the structure. This is possible because discontinuities in a structure will produce detectable AE before structural failure occurs. The AE technique is considered in this thesis. The AE are transient elastic waves that are primarily generated by microcrack growth. Hence the analysis of AE produced during mechanical tests is a non-destructive technique for the study of the health of structures.

Sensors are a critical component in a SHM system. They play the part of the ears and eyes of the system. This thesis deals not only with developing a monitoring system but also focuses on active materials for building sensors for monitoring of structures. Active fibers composites (AFC) were first manufactured in 1999 at MIT [1] and mainly focused primarily on the actuation properties of the AFC. The idea of a composite material consisting of an active piezoceramic fibrous phase embedded in a polymeric matrix phase has many advantages.

Typically, crystalline materials have much higher strengths in the fiber form, where the decrease in volume fraction of flaws leads to an increase in specific strength. Also, in addition to protecting the fibers, the flexible nature of the polymer matrix allows the material to more easily conform to curved surface found in realistic industrial applications. Moreover, active fiber composites offer many distinct advantages with respect to their monolithic counterparts. The multiphase construction yields a more robust actuator that is capable of being added to a lay-up as “active layers” along with conventional fiber-reinforced laminae. While complex arrangements of piezoelectric

blocks are required to sense the bending and twisting of a structure, the fiber-reinforced composite nature of active fiber composites yields in-plane sensing or anisotropy, allowing a single patch the ability to sense both bending moments and twisting torques. Also the AFC have a large bandwidth ranging from 1 Hz into MHz. All these characteristics of the AFC make them well suited for realistic monitoring applications. These AFC form the artificial nerve's of the Structural Neural System (SNS). These are tested in the Smart Structures and BioNanotechnology laboratory [4] and the results are discussed in results chapter-7 of the thesis. Research on the use of a SNS is reported in papers published by Schulz et. al [8-11]. This initial research showed that the SNS allows efficient use of data acquisition instrumentation for structural health monitoring. The Sensor/Neuron measures dynamic strains and these signals are interpreted to indicate if the structure is operating within the limits of the design specifications. The SNS is a biomimetic concept, which is analogous to that of the human neural system. The small size sensors coupled with large coverage will provide the simplicity and sensitivity needed for real time structural health monitoring. The goal of this research is to develop a passive SNS based on the architecture of the biological neural system using smart sensors and electronic components to detect AE due to propagating damage. The SNS reduces the number of data acquisition channels and simultaneously improves the sensitivity of damage detection. This thesis specifically deals with development and testing of a prototype two neuron SNS [6]. It carries further the work done previously in Smart Structures and Biotechnology laboratory [4]. The experimentation was conducted on an Aluminum beam and a glass fiber composite plate. The results of the testing are discussed in the thesis which show that the automated SNS developed in the lab was

sensitive to low frequency dynamic strains caused by structural vibrations and impact and high frequency AE that accompanies damage growth [52]

1.2 Piezoceramic Material

Piezoceramics are a type of active material which functions as an energy conversion device, transforming an energy input of one form into an energy output of another form. In this sense, a variety of materials qualify as active materials other than piezoceramics, including shape-memory alloys, electroactive polymers, and magnetorheological fluids. Each of these materials accepts one type of input field and outputs a field of another form. Table 1.1 shows the behavior of each of these active materials.

Material	Input Field	Output Field
Piezoceramic	Voltage	Displacement
Shape Memory Alloys	Temperature	Displacement
Electroactive Polymers	Voltage	Displacement
Magnetorheological fluids	Magnetic Field	Viscosity

Table 1.1 Behavior of various Active Materials.

Over the past 20 years a great amount of research has been done in the field of smart materials especially in the field of piezoceramics. When a voltage stresses a piezoceramic element electrically, its dimensions change. Figure 1.1 shows a monolithic piezoceramic patch. When a force stresses the monolithic PZT mechanically, it generates an electric charge. If the electrodes are not short-circuited, a voltage associated with the charge appears. A piezoceramic is therefore capable of acting as either a sensing or transmitting element, or both. Since piezoceramic elements are capable of generating very high

voltages, they are compatible with today's generation of solid-state devices - rugged, compact, reliable, and efficient. Pierre and Jacques Curie discovered piezoelectric materials in the form of quartz, tourmaline and Rochelle salts in 1880 as a result of their investigations of pyroelectricity [12]. Polycrystalline, metallic compounds, piezoceramics exhibit extremely strong electromechanical coupling and mechanical properties similar to other ceramic materials. A flurry of improved piezoceramics exhibiting stronger piezoelectric effects were developed over the course of the next two decades, yielding the most common modern piezoceramics like Lead Zirconate Titanate (PZT) and Lead Metaniobate (PMN).

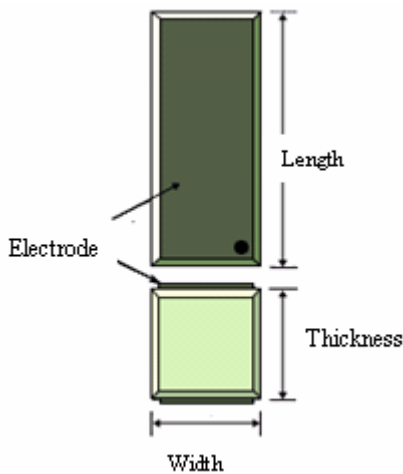


Figure 1.1 Monolithic PZT patch [9]

1.3 Interdigitated Electrode Monolithic Ceramics

The interdigitated electrode concept was introduced to enhance performance of monolithic ceramic actuators [14] which is shown in Figure 1.2.

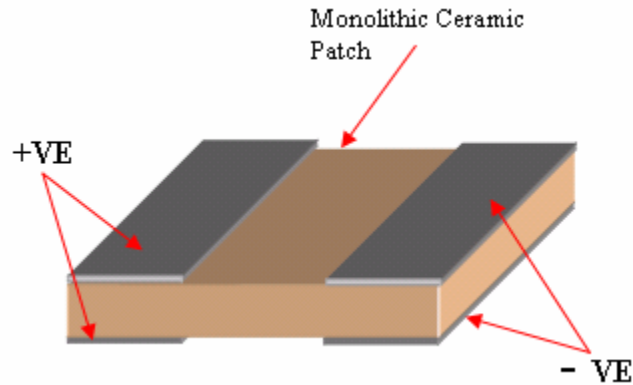


Figure 1.2 Interdigital Electrode Monolithic Ceramic [15]

The electrode fingers of alternating polarity are arranged on the top surface and a mirror image is on the bottom surface. The electric field is thus aligned in the plane of the ceramic. The advantage of this technique was the use of the higher primary piezoelectric effect (d_{33}) and anisotropic actuation and sensing. Even though the use of a higher electromechanical coefficient (d_{33}) gave some advantage over the monolithic PZT the problems associated with catastrophic cracking of monolithic ceramics still remained. Micro cracks initiated near the electrodes leading to crack propagation and failure of actuator/sensor under stress. This initiated a number of new electroding schemes like floating electrodes but there has not been a permanent solution to the problem.

1.4 Piezoelectric Active fiber composite

Piezoelectric fiber composite actuators were originally developed as a means of overcoming many of the practical difficulties associated with using monolithic piezoceramic actuators in structural control applications [6]. Chief among these difficulties were brittleness of piezoceramic materials, poor conformability, particularly when applied to non-planar structures, nondirectional nature of strain actuation, and

overall low strain energy density. In these the piezoceramic fibers were unidirectionally aligned to maximize the volume fraction and anisotropic actuation. Uniform electrodes were applied through vapor deposition above and below the ceramics. The poling direction was through the thickness and actuation was due to the transverse piezoelectric effect. There were certain benefits from the standpoint of actuation such as strength and conformability, performance and large-scale actuation. At the same time there were problems associated with the dielectric mismatch between the fiber and matrix material, which limited the actuation energy density. There was no investigation of the use of these materials from a sensor perspective. For sensor applications, the bulk PZT material was used. One of the disadvantages of the active fiber composite was the high cost fabrication process.

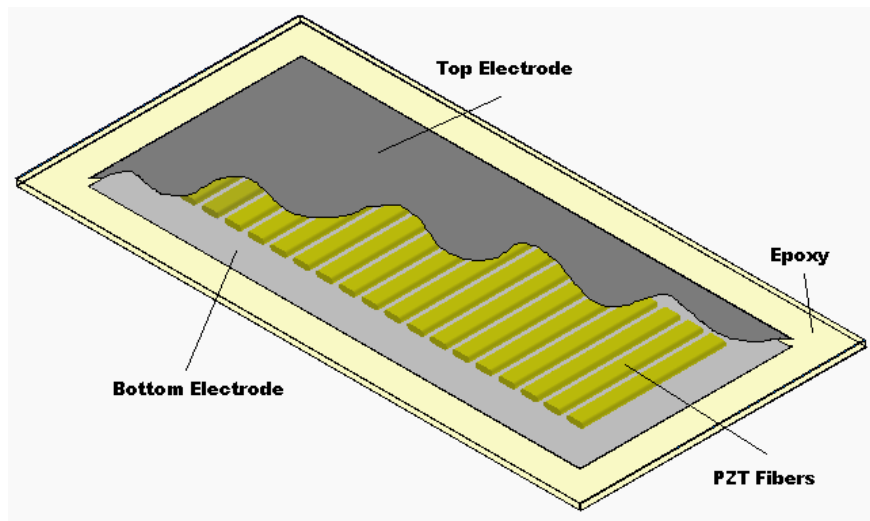


Figure 1.3 Piezoelectric Active Fiber Composites [9]

1.5 The Macro fiber composite

The NASA Langley Research Center Macro-Fiber Composite (MFC) actuator [16] was developed to alleviate many of the manufacturing and performance disadvantages

associated with early piezocomposites [6]. The MFC (see Figure 1.3) retains the most advantageous feature of the early piezocomposite actuators, namely, high strain.

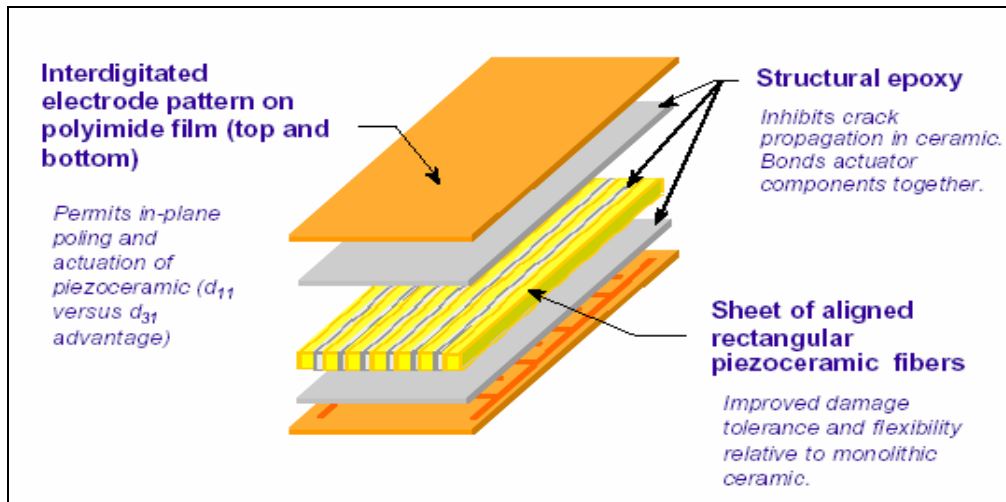


Figure 1.4 Components of Macro Fiber Composites [K. Wilkie, 14]

The MFC used low cost piezoceramic wafers, which are machined using a computer controlled saw. The piezo sheets are easy to handle and are precisely aligned in the epoxy matrix within the actuator package. Just as was the case for Active Fiber Composites, MFC^s use an interdigitated electrode pattern to deliver an electric field along the length of the fibers and rely on solid bonding between the matrix and fibers to properly transfer actuation loads. There was no work on the MFC materials from the sensor perspective.

1.6 Continuous Sensors

AFC nodes can be connected in a series arrangement to form a continuous sensor or Active Fiber Sensor (AFS) [17-20]. This resulted in a reduction in the number of data acquisition channels for AE monitoring and a larger structural area could be monitored using continuous sensors. In addition to this, the probability of the sensor being close to

the damage increases resulting in better diagnostic characteristics. This is essential for composite structures where waves generated by acoustic emissions attenuate rapidly. With the continuous sensor arrangement, a large number of sensors can be connected in a series arrangement requiring only one channel of data acquisition. Any damage event producing an AE signal near any node on a row of the sensor will generate a response. If this arrangement is used to form a grid of sensors, responses from rows and columns can be used to locate the cell within which the damage event has occurred.

1.7 Objective of the Research

The Objective of this research is to understand the characteristics of an active fiber composite and its use in structural health monitoring for sensing applications. This thesis focuses on the relationship between sensing systems and their ability to detect changes in a structure's behavior. The recent development in active fiber composites has been a driving factor in developing a unique approach using the AE technique. This thesis explains conceptually the development of single fiber AFC sensors using PZT ribbons. The modeling and constitutive relations of the AFC and continuous sensors are also explained. The manufacturing of the AFC sensors in the Smart Structures and Bionanotechnology lab [4] is given in detail in chapter 4 of the thesis. In this thesis a data acquisition system is developed for processing of the acquired data using LabVIEW and incorporating single fiber continuous sensors in the structural neural system (SNS). The testing indicates that the SNS will be able to continuously monitor a structure and provide a long-term history of the health of the structure. Initial testing with conventional monolithic PZT is done to understand the PZT behavior and verify the feasibility of the SNS system developed for structural health monitoring using AE techniques. Further an

effort is made to understand the behavior of the AFC for different excitations like low frequency tapping, a lead break and sinusoidal actuation using the function generator. In

brief the thesis covers the following aspects

- Tries to understand concepts of active fiber composite
- Models and forms the constitutive relations of AFC
- Gives in detail the manufacturing process for the AFC
- Develops a data acquisition system using LabVIEW for acquiring and processing the data
- Characterizes the manufactured AFC

Chapter 2 Active Fiber Composites

This chapter discusses in brief piezoelectric active fiber composites, their design, modeling and the steps that are necessary to manufacture them. This chapter deals with the overall choices that were made in selecting different materials from a manufacturing point of view while keeping in mind the functional requirements of the sensor. Various tradeoffs were investigated regarding the manufacturing and the performance of the AFC sensor. The design had the following specific objectives:

- To explore the sensitivity issues and tradeoffs in the design process of an active fiber sensor.
- To determine a set of material combinations which will satisfy the sensor requirements
- Illustrate a single design iteration through a decision making process
- To develop a general approach for future design of active fiber sensors

AFC combine piezoceramic materials and additional inactive components in a specific structure to form an overall actuator/sensor package with the advantageous properties of both piezoceramics and other structural materials. The advantages are:

- Greater flexibility in design, handling and application
- Unidirectional sensing, mostly self-powered
- More rugged than monolithic PZT
- The electroding can be designed for the application
- Fiber preforms can be cut to different shapes easily
- A high bandwidth and high voltage coefficient for sensing acoustic waves

This chapter is divided into different sections that elaborate the design issues in the process of development of active fiber sensors. In the end the current design procedure that is being used is summarized.

2.1 Modeling Active Fiber Composite Sensors

Modeling of the AFC sensor is discussed briefly here. The linear constitutive relationship is used to relate mechanical and electrical fields. The piezoelectric constitutive equations are listed in the IEEE standard ANSI/IEEE Std. 176-1987. This standard is used to derive the basis of the AFS electrical modeling.

When a PZT material is subjected to mechanical stress ‘T’ with units Newton per meter squared $\left(\frac{N}{m^2}\right)$ it produces an electric displacement ‘D’ with units of Coulomb per meters squared $\left(\frac{C}{m^2}\right)$ which is a linear function of ‘T’ written as $D = dT$ where d is the Piezoelectric coupling coefficient with units of Newton per Coulomb $\left(\frac{N}{C}\right)$. When an electric field ‘E’ with units of Volts per meter $\left(\frac{V}{m}\right)$ is applied across PZT electrodes it produces a strain or distortion ‘S’ which is given by $S = dE$. For an elastic material the relationship of strain ‘S’ to stress ‘T’ is given by $S = s^E T$ where s^E is the mechanical compliance of the material at zero mechanical stress with units of meters squared per Newton $\left(\frac{m^2}{N}\right)$. For a dielectric material, the electric displacement ‘D’ and electric field ‘E’ are related by $D = \varepsilon E$ where ε is the dielectric permittivity measured at zero

mechanical stress with units of Farad per meter $\left(\frac{F}{m}\right)$. For a piezoelectric ceramic these relationships are given by the following equations [28].

$$S_i = S_{ij} T_j + d_{mi} E_m$$

$$D_n = d_{nj} T_j + \varepsilon_{nm}^T E_m$$

where $m, n = 1, 2, 3$ and $i, j, k = 1, 2, 3, 4, 5, 6$. The piezoelectric

constitutive equation in matrix form can be written as:

$$\begin{bmatrix} D \\ S \end{bmatrix} = \begin{bmatrix} \varepsilon^T & d \\ d_t & s^E \end{bmatrix} \begin{bmatrix} E \\ T \end{bmatrix} \quad (2.1)$$

Equation (2.1) is a coupled field equation that relates the applied electric field $(E)_{3 \times 1}$ in Kilovolts/meter, the electric displacement $(D)_{3 \times 1}$, the strain $(S)_{6 \times 1}$ and the stress $(T)_{6 \times 1}$. Material properties such as the dielectric permittivity $(\varepsilon^T)_{3 \times 3}$, the induced strain $(d)_{3 \times 6}$, and the compliance $(s^E)_{6 \times 6}$ are used to relate the mechanical and electrical fields. The subscript ‘t’ indicates transpose and superscript ‘T’ indicates a constant stress condition. In the continuous sensor arrangement the sensor can be modeled as a capacitor in parallel with a current source [17-19]. Further simplification is possible in beam case if the electric field is only applied in 3-direction and any actuation transverse to the AFC fiber direction is neglected, then the one dimensional equation can be used assuming that the PZT ribbon fibers exhibit linear bulk piezoceramic properties. If the sensor is bonded perfectly to the structure, then the strain/displacement compatibility and stress/force equilibrium principles can be applied. With an assumption that in vibration of a simply supported beam strain occurs only in the 1 direction and the AFC is poled in 3 direction, equations (2.1) reduces to:

$$S_1 = s_{11}^E T_1 + d_{13} E_3 \quad (2.2)$$

$$D_3 = d_{31} T_1 + \varepsilon_{33}^T E_3 \quad (2.3)$$

Rearranging the above equations and using the relation $e_{31} = d_{31} / s_{11}^E$ and $d_{13} = d_{31}$ gives:

$$D_3 = e_{31} S_1 + \varepsilon_{33}^S E_3 \quad (2.4)$$

The current $i = \dot{Q} = \dot{D}_3 A_e$ and $E_3 = V / A_e$ where Q is the charge, A_e is the electrode area, and $\varepsilon_{33}^S = C_p h_e / A_e$ where C_p is the capacitance and h_e is the electrode spacing. This gives:

$$i = e_{31} A_e \dot{S}_1 + C_p \dot{V} \quad (2.5)$$

and for open circuit case where $i=0$;

$$V = e_{31} A_e S_1 / C_p + V_0 \quad (2.6)$$

Here V is the voltage generated by the AFC sensor in the dynamic strain condition and V_0 is the initial voltage. These equations can be used to approximate the d_{31} coefficient by having a single AFC sensor bonded on a beam when a known load and loading cycle is applied to the beam. The response from the sensor can be measured using an oscilloscope. This is the simplest way to evaluate the approximate properties of the manufactured.

2.2 Design of Active Fiber Composites

The design adopted here is a result of initial design iteration using available resources. Further experimental evaluations and availability of new materials will help adapt new models and design improvements.

The following flowchart shows in brief the steps necessary for active fiber sensor design which is discussed later on.

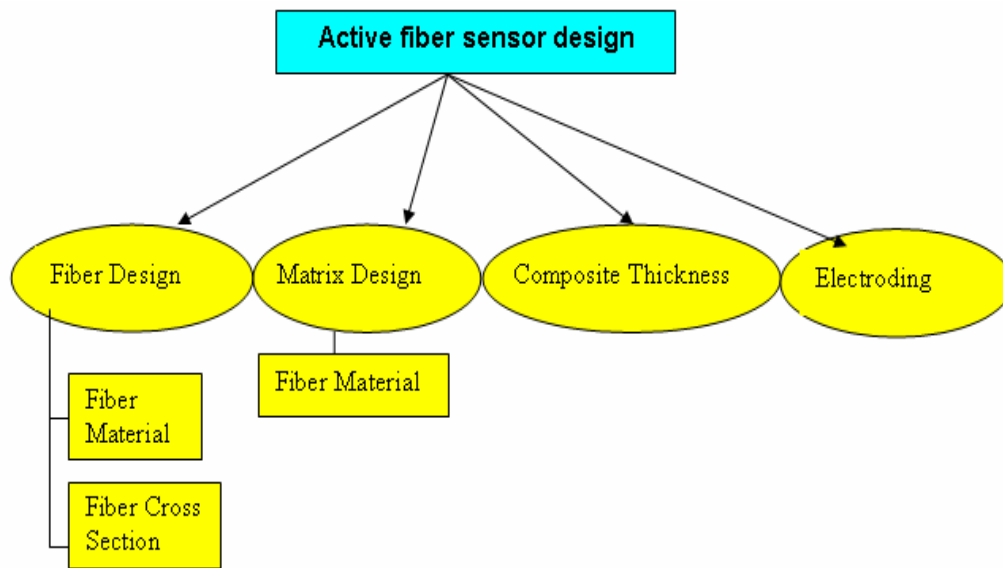


Figure 2.1 Flowchart of Active Fiber Sensor Design

2.3 Fiber Material

The properties of different PZT materials available are given in the Table 2.1. The comparisons are based on the one-dimensional mode of operation. The PZT 5H has a very high induced strain constant due to domain mobility and also has the highest induced stress constant. This property makes the material very suitable for actuation applications; the good actuation capability is also evident in the high coupling coefficient that takes into account the dielectric constant. In general such hard ceramics are suitable

	PZT 5A	PZT 5H	PZT 4S	PZT 8M
Dielectric K_{33}^T	1770	3350	1500	800
Induced Strain d_{31} (m/V)	171	292	123	-97
Induced Stress e_{33} (N/C)	15.8	23.2	14.6	17.3
Coupling Coefficient k_{33}	0.774	0.790	0.861	0.767
Young's Modulus (GPa)	53	48	60	77
Depole Stress T_{33} (MPa)	72	44	>150	>150
Coercive Field (kV/m)	11.2	7.2	8	8.4

for actuation applications. For sensor application a softer ceramic with a similar coupling coefficient is required for an efficient conversion of mechanical energy into electrical energy. The results of actuation and sensing capabilities of the manufactured AFC are discussed in chapter 6. The choice of material is also dependent on the ease of polarization, handling and availability in the form of fibers. The fibers used in the research were commercially produced by CeraNova Corporation [22]. This company has been involved in manufacturing PZT fibers since 1992 and has produced all the ribbon fibers used in this research.

Table 2.1 Comparison of one dimensional properties of PZT ceramics [15-16]

The fibers used are PZT 5A ribbons bought in approx. 6 inches length and approx 250-micrometer height and 750-micrometer width (i.e. 3:1 aspect ratio).

2.4 Fiber cross section

The piezoelectric ceramic fibers are available in different cross sections as shown in Figure-2.2

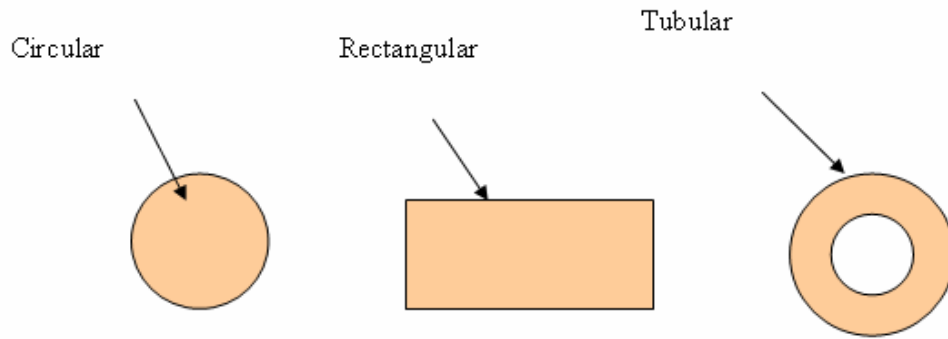


Figure 2.2 Types of PZT fibers

Rectangular fibers have certain advantages over the circular ones. Fibers with a rectangular cross section have a higher thickness fraction of piezo ceramic material for the same thickness of the composite (diameter in circular fiber case). A higher thickness fraction of ceramic material is desired for maximum sensitivity. Also rectangular fibers show more efficient use of matrix material. The surface area coming in contact with electrode is also higher in fibers with rectangular cross section. The choice of fiber cross section also depends on application. If we normalize performance of fibers with their mass for a given volume of composite the apparent advantage of rectangular fibers reduces. In the current use for sensing the high frequency low amplitude AE, the sensors should be small in size and more sensitive. These requirements make rectangular fibers an obvious choice. The rectangular fibers are easier to handle so the decision was made to use these fibers for development of sensors.

2.5 Composite thickness

Once the fiber cross-section is determined the next step is to determine the thickness of the composite ply. The fibers used have a thickness of 250 micrometers so the overall thickness of the composite ply was kept as close to that number as possible. To have maximum wetting of fibers by epoxy and avoid any voids, a pressure-casting mold was used to make the composite ply. Any increase in the thickness of the ply will require a higher poling voltage. The process of manufacturing the sensor requires removing excess epoxy from top and bottom of the fibers after the poling. After removal of excess epoxy another layer of conductive epoxy is applied which acts as an electrode as well as a bond with the structure. Since the electrodes are directly in contact with the AFC matrix, the sensitivity is improved.

2.6 Matrix Material

The matrix material surrounds the fibers and provides the structural integrity for the sensor. In order to do that the matrix material should form a good bond with the PZT ribbon fibers. In the longitudinal direction the strength of the active fiber composite is determined primarily by the strength of fibers but in the transverse direction it is determined by the bond between the fiber and epoxy and by the strength of epoxy itself. The performance requirement for the matrix material apart from the strength is to have a high dielectric breakdown so that it can survive high poling voltages. Also the matrix material should not have high porosity which might cause arcing between the electrodes during poling or cause percolation of conductive epoxy at the stage of electroding. During the initial design iterations silver conductive paint was used to paint electrodes on

the sensor due to ease of use. It was observed in many sensors that the paint percolated through the epoxy matrix material and caused electric short circuit between the electrodes. The stiffness of the matrix material is expected to affect the unidirectional sensing characteristics of sensors. Based on the on the earlier experimental work done in Smart Structures and BioNanotechnology lab [4] a selection of EPON Resin 862 epoxy was made for the matrix material [17].

2.7 Electroding

In active fiber sensors electrodes are needed to collect the charge generated by the piezo ceramic fibers and to provide connection for completing the electric circuit. Electrodes are also needed to create the strong electric field required for alignment of electric dipoles during the poling process. The two requirements are different from each other by way of voltages involved and the requirements of sensing itself. The Poling process is done prior to the use of the active fiber composite as a sensor. Poling through the thickness can be achieved by simply placing an electrode on top and bottom of the composite and applying a high voltage using an amplifier. Due to the high resistance of the matrix material the current drawn will be negligible. An unique approach was used to apply a temporary electrode made of strips of copper for poling and then replace the electrodes with the final electrodes. It was observed in the initial design iteration that if copper strips are kept in the final assembly the strain transfer from the structure to the piezo fibers reduces considerably during sensing. This result in a very low response from the sensor and the waves generated by small acoustic emissions are not detected. The problem was solved by using conducting silver epoxy H20E as the final electrode. The advantage in this approach is that the epoxy forms a good bond with the active fiber

composite and at the same time it can be used to bond the whole sensor to the structure if needed. This eliminates a few layers of material like a metallic electrode, insulating film and an additional layer of glue that should be used in conventional sensors. This provides the maximum sensitivity of the active fiber sensors. The properties of conductive epoxy H20E are given in Table 2.2 (courtesy Epoxy Technology, INC.) which is given in detail in Appendix E.

Parameter	Typical Value
Number of Components	Two
Mixing Ratio	Part A : Part B :: 1:1 by weight
Cure Schedule	80 ⁰ C 90 minutes
Viscosity	2200-3200 cPs
Glass Transition Temperature	> 80 ⁰ C
Lap Shear Strength	1500 psi
Die Shear Strength	> 10Kg / 3400 psi
Degradation Temperature	410 ⁰ C
Thermal Conductivity	29 W / m ⁰ K
Volume Resistivity	< 0.0004 ohm-cm
Pot Life	4 days
Shelf Life	One Year

Table-2.2 Typical Properties of the conductive epoxy H20E (courtesy Epoxy Technology, Inc.)

2.8 Summary

This chapter discussed a number of issues in the design of active fiber composites using different constituent materials. The design studies demonstrated the tradeoffs with material selection, which often involves conflicting choices for the optimal solution. Such a conflict exists with fiber material selection, where hard ceramics seem best suited for low field response and high stress designs, but soft ceramics are the material of choice for high field actuation. The chapters-2 and 6 involve manufacturing and testing of the active fiber sensors.

Chapter 3 Manufacturing of Active fiber Sensors

The next logical step after the design of the AFC sensor is the development of the manufacturing technique. During this step the practical limitations in the theoretical design along with the material limitations were understood resulting in various iterations before finalizing a general manufacturing approach. For example, finding a gasket material which will give the right thickness of the composite. Also as the gasket gets compressed in the mold, the reduction in thickness was needed to be accounted for before choosing the gasket material. One of the other factors was the fiber geometry which did set the maximum compaction and maximum composite size. In developing the techniques for manufacturing, it is also possible to come across innovations that could improve the design.

The initial iteration was based on the previous work that was carried out in the Smart Structures and BioNanotechnology Lab [17,4]. The initial iteration which lacked geometrical uniformity and repeatability in composite properties was improved. Much of the difficulty was related to the alignment of the fibers and the excessive composite thickness necessitating sanding of the composite prior to electroding, causing difficulty in these areas. However, this initial work had identified many of the issues with manufacturing methods, and laid the groundwork for the methods presented in this chapter. Previous work carried out in the Smart structures and BioNanotechnology lab [4] consisted of six ribbon fiber of shorter length. This chapter describes new manufacturing techniques that accommodate the change in geometry and the single neuron sensor. The chapter describes in detail the steps that are taken for successfully manufacturing the AFC sensor.

The following are the key parameters, which had to be controlled while manufacturing of the Active fiber sensor.

Voids

Voids are the cavities or the surface holes found on the surface or inside the composite casting where air or vacuum is trapped in the matrix. Figure 3.1 shows the void formation during the casting of the AFC sensor. Castings with a significant number of voids must be discarded, resulting in wasted product, time and labor. Voids create a concentration of electric field in this area. Therefore it is necessary and important to understand the causes of voids and what can be done to minimize them. This is the first step to a more efficient and productive in casting operation.

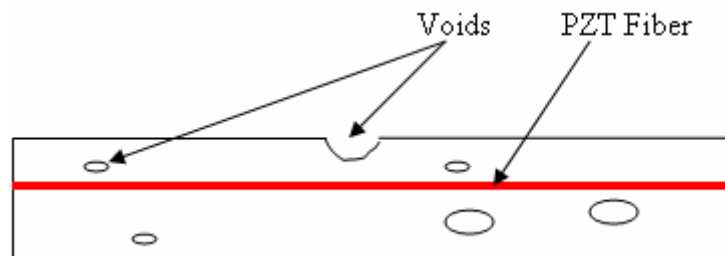


Figure 3.1 Void formation in AFC preform

Voids are attributed to following factors:

- Release agent
- Air

The following information has been compiled through the preliminary manufacturing of composites. Some of the techniques found here are the results of many years of research and development. To minimize voids a careful preparation of the epoxy and application of release agent is necessary which is explained in the following sections.

Alignment

Alignment of the PZT fiber is very necessary before injection of the epoxy in the mold. Two AFC preforms can be cast at the same time. Therefore it is necessary that the fibers of each preform maintain their position during the period of injection of epoxy and curing. Any misalignment may result in touching of the PZT fibers thus weakening the sensor. To achieve proper alignment, a double stick tape is used which is explained in later sections.

Compaction

Compaction plays a very important role in deciding the thickness of the AFC sensor. Increase in the thickness of the AFC preform results in higher poling voltage. Ideally the thickness of the preform should be equal to the thickness of the PZT fiber (0.25 mm) however the thickness of the AFC preform is determined by the thickness of the Gasket used. Different materials of gasket were tried like polycarbonates, Teflon, paper etc. Within the available materials the paper gasket gave the minimum thickness (0.30 mm) which was used for casting of the AFC sensors.

3.1 Mold

The PZT ribbons need to be placed in an epoxy medium in order to remain at equal spacing and provide strength to the preform. The mold that is used for the casting of the AFC had the following requirements:

- Accommodate the long AFC neuron
- Develop compressive pressure on the gasket
- Withstand temperatures up to 600⁰F
- Be easy to clean

Using these basic guidelines a pressure mold was manufactured in the UC machine shop. The various parts of the mold are shown in Figure 3.1 and are described below along with their functions.

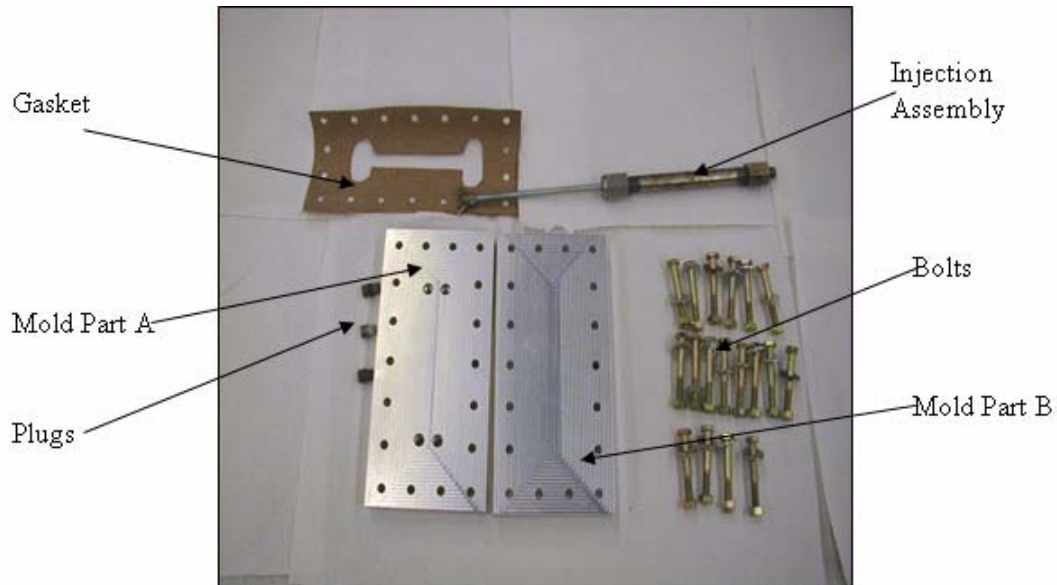


Figure 3.2 AFC casting Mold

Mold Design, Part A/Part B

Part A and Part B are manufactured from Aluminum 7051 bar stock. The overall dimension of each part is 7" X 3.5" X 0.75". Part A has four threaded holes on it. One for injecting the epoxy and three for venting which are plugged after the injection of epoxy is over. There are in all a total of 18 bolt holes on Part A and Part B which are used to hold them together and develop compressive pressure on the gasket.

Gasket

The gasket used is an automotive paper gasket which is used in car engines. The gasket is cut out using a razor blade for each casting. The cut area is dog bone shaped in which the single fiber neuron is aligned. The size of the cut area is such that it

accommodates two neurons at a time thus enabling the casting of two neurons in a single batch.

Injection Assembly

The injection assembly shown in Figure-3.3 consists of:

- Injection cylinder
- Nipple
- Collar
- Piston rod
- Piston
- O-rings



Figure 3.3 Injector Assembly

The whole injection assembly is made from standard parts except for the piston, which is custom manufactured. The length of the cylinder is based upon the volume of epoxy that needs to be injected in the mold.

Bolt/Plugs

There are total of 18 bolts, which are used to assemble the mold and develop compressive pressure on the gasket thus reducing the thickness of the sensor. Plugs are used to plug the venting holes in Part A.

3.2 Manufacturing process

The manufacturing of AFC can be divided into

- Casting
- Poling
- Electroding

3.2.1 Casting

Casting is the most important step of all. Casting is described in detail below.

Cleaning the mold and injector

The mold and the injector are cleaned using cleaner 19 SAM manufactured by AXEL industries to remove any dirt or deposits from previous casting. They are then cleaned using acetone and are blow-dried using compressed air.

Treating the PZT fibers

The PZT fibers are the sensing element in the AFC. These ribbons are PZT 5A fibers with an aspect ratio of 3:1. Since they are brittle, they can easily be cut with a razor blade to the appropriate length for use in the molding process. The piezoceramic ribbon fibers shown in Figure 3.4 are 165.1mm long so they are cut into 100mm long pieces using a sharp razor blade. The fibers are cleaned by immersing them in an acetone bath for

15mins and then they are blow-dried using pressurized air. Finally they are heated for 15 minutes at 200° F.

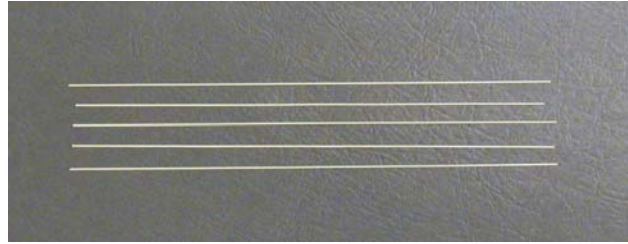


Figure 3.4 PZT fiber size $165.1mm \times 0.75mm \times 0.25mm$ [23]

Applying release agent

Three coats of release agent are applied. After application of every coat it is allowed to dry for 15minutes. Applying release agent is a very important step in casting of the AFC. Release agents act as a "lubricant" between the mold and the epoxy itself. The proper application of a release agent will yield castings without surface voids. However, when a release agent is over applied, it may "pool" or "puddle" on the mold. As the epoxy is injected into the mold these pools prevent the epoxy from filling in all the detail. When the casting is removed from the mold surface voids will be apparent in the areas where pooling occurred. Voids caused by too much release agent are recognizable as small spherical voids on the surface of the finished casting.

Aligning the fibers

Misalignment results in bidirectional sensing of the AFC sensor. Therefore it is necessary to properly align the fibers. The fibers are dipped in the epoxy and are manually aligned on the Part A of mold. The mold is then heated at 200 F for 10 minutes till the epoxy gets tacky. This prevents the fiber from moving during the injection process

thus maintaining the alignment. Using a double stick tape is another way to align the fibers.

Preheating the Mold and injection assembly

The Part A and Part B are assembled along with the gasket using the bolts. The mold along with the injection assembly is preheated to 100F, which is necessary for maintaining low viscosity of the epoxy while casting.

Preparing the epoxy

During casting the epoxy matrix surrounds the ribbon fibers. Approximately 24.2 grams of EPON Resin 862 epoxy is taken in a beaker. It is then heated in a vacuum oven for 10 minutes at 100°F under vacuum. This helps in degassing and decreasing the viscosity of the epoxy. This procedure usually takes about 15 minutes and is a critical step in casting. If this step is eliminated then the preform becomes porous because of the tiny air bubbles trapped inside the epoxy matrix

Injection of epoxy

To inject and monitor the flow of epoxy four holes were made on the surface of the top-mold. One of these would be used to inject the epoxy and the other three are monitored and closed in consecutive order based on the location of these holes. The epoxy filled injector is then assembled to the mold. The threaded piston rod is then turned to inject the epoxy in the mold. As the epoxy reaches the hole it starts flowing out through it. Plugs are used to plug these holes. This method serves as a tool to monitor the distributed flow of epoxy through out the mould. Once all the holes are plugged, the injector's screw should be turned 13 full turns in order to create a pressure of approximately 350 PSI.

3.2.2 Curing

The assembly (Mold + injector) is heated in a Fisher scientific vacuum oven at 180° F show in Figure 3.5 for approximate 120 minutes. At the end of the process the mold is allowed to cool down to room temperature



Figure 3.5 Curing for the AFC Sensor

After cooling, the thin wafer of preform can be removed from the mold by cutting off the ends just inside the injection holes using a razor blade. Each preform can be used to produce sensor with length varying from 1”- 4”.

3.2.3 Electroding

Electrodes are necessary as they serve following purpose:

- Helps in poling to perform
- Forms electrical lead from the sensor

In order to save costs, a successful method was developed to place the electrodes on the small 4” long AFC sensor using conventional tooling. The Table 3.1 shows the mechanical tolerances of the AFC preform that were manufactured.

Dimension	Units	Tolerances
Length	75mm-80 mm	+/- 2 mm
Thickness	0.30 mm to 0.32mm	+/- 0.02 mm
Weight	0.36 gm	+/- 0.05 gm

Table 3.1 Manufacturing Tolerances for an AFC preform

Two possibilities were tried for electroding:

- Structure Integrated electroding
- Stand-alone electroding

In either case silver conductive epoxy is used (Appendix E) to form the electrical contact. A copper strip or electrical wires are integrated in the silver conductive epoxy during curing to form the electrical leads from the sensor. Depending on the application these sensors can be made stand alone sensors or sensors which can be integrated in the structure itself. The later being more convenient and practical as far as the installation part goes. Both types are discussed here in brief however the stand alone electroding is used for general purposes.

Structure integrated electroding

The sensor is bonded with the help of silver conductive epoxy which forms the electrical leads for poling and acquiring the response of the sensor after its mounted on the structure as shown in Figure 3.6. The processes of curing, bonding and poling etc are carried out on the structure itself, a Kapton[®] sheet is not used. Even though this helps in

better strain transformation from the structure to the sensors due to practical reason it may not be feasible for large structures or on metallic structures.

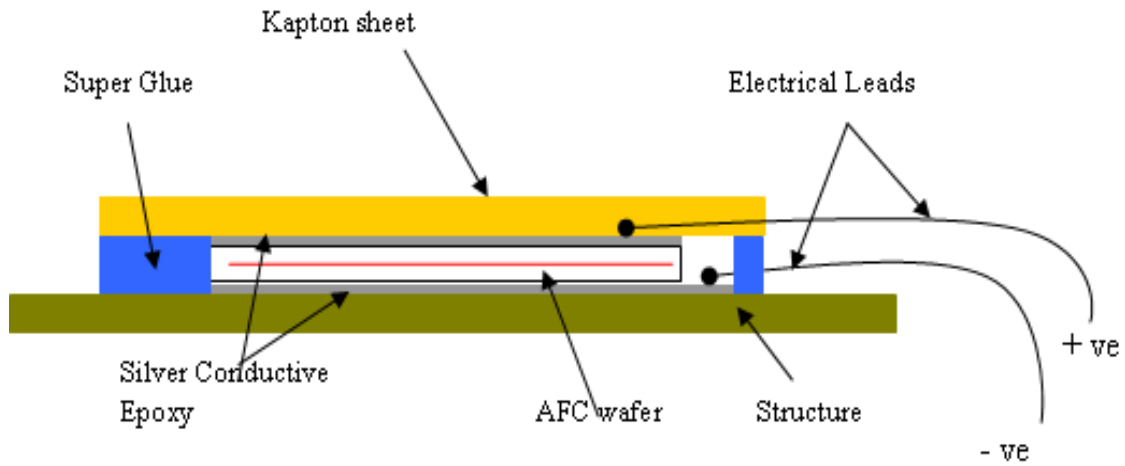


Figure 3.6 Structure Integrated electroding

Stand-alone electroding

The sensors are bonded on a Kapton[®] sheet away from the structure as shown in Figure 3.7. The process of poling and curing is done in laboratory environment. The sensor (encapsulated in Kapton[®]) is bonded according to the procedure explained in Section 3.3.4.

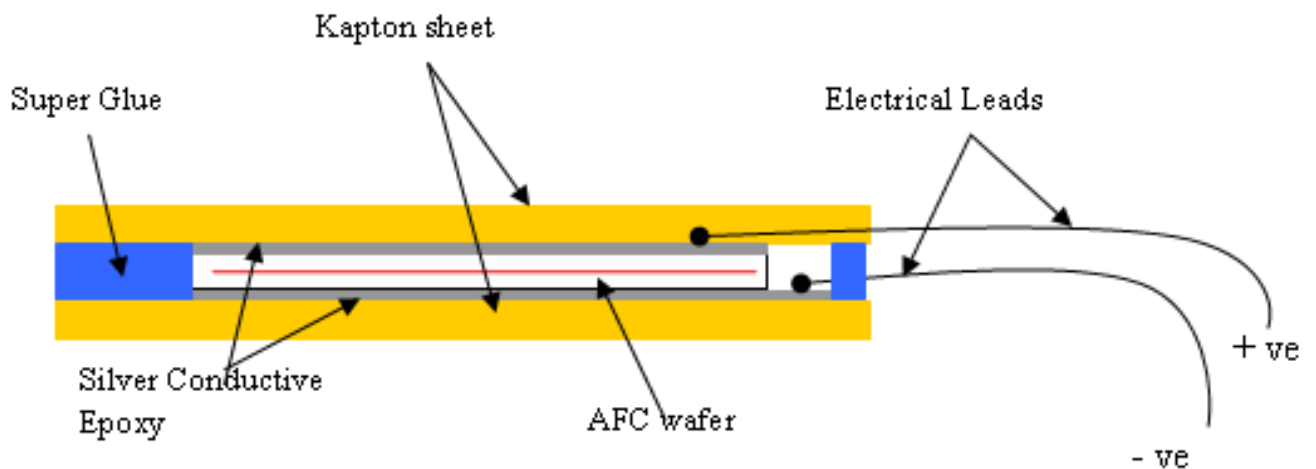


Figure 3.7 Stand-alone Electroding

3.2.4 Field Installation Procedure

Sensors installation is an important step in structural health monitoring that may have significant impact on the nature of data that is collected. The development of an installation method which was not only reliable but also repeatable was necessary and also which would reproduce the same results. For this a literature survey was done and from the published data an initial approach was formulated. The way in which the sensors are installed depends on the type of structure. It is known that the PZT sensors can produce voltage as high as 1000 V. For this reason it is very important that the PZT sensors must be isolated from the metallic surface. The operating temperature range of Epon 862 limits the temperature range in which the Active fiber composite sensors operate, which is from -60°F to $+200^{\circ}\text{F}$. Also the active fiber composite sensors must be capable of being installed in the field on surfaces where access is difficult and the time available for installation is limited. Imbedding active fiber composite sensors in the structural component is possible, but the structural integrity of the smart material (active fiber sensor) is difficult to verify over the component's life.

Commercially available monolithic PZT patches have a polyamide coating and wire connector to make installation easier. However the Active fiber composite sensor built doesn't have a polyamide coating nor wire connectors. These need to be built into the sensor while bonding (for composites) or before bonding (for metallic). With keeping all these factors in mind a field installation procedure was developed which is shown in Figure 3.8

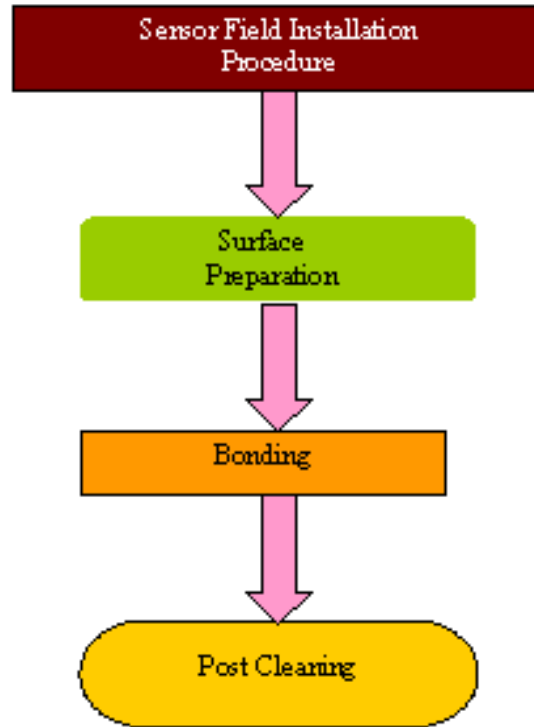


Figure 3.8 Sensor field installation procedure

Key steps for quality bonding

Surface Preparation

All foreign materials, such as dirt, grease, cutting coolants and lubricants, water or moisture, and weak surface scale (e.g., oxides, sulfides), must be removed. Thorough cleaning with various physical or chemical processes removes these contaminants and conditions the surface for bonding. The process of cleaning the surface usually involves several of the following steps:

- Solvent Cleaning
- Mechanical Cleaning

Solvent Cleaning

Clean the application area of the AFC sensor element with cotton tipped applicators dipped into a solvent, e.g., Acetone (do not use cotton buds with plastic grip). Renew the cotton tips frequently until the application surface is completely clean (cotton tips remain clean). If possible, the surface area cleaned should extend beyond the space required for the Active fiber sensor. The same procedure needs to be followed for the Active Fiber Composite sensor.

Mechanical Cleaning

Surface abrasion (with abrasive paper) is a common procedure in preparing metals or composites for strain gage bonding. The same procedure is used for AFC sensors. Surface abrasion can be used on plastics and composites, but should always be preceded by degreasing to prevent embedment of contaminants in the surface. For some high-performance composites, however, abrasion may not be permitted because of the risk of damage to near-surface fibers. Moreover, abrasion is not always adequate with certain types of plastics (e.g., fluorocarbons, polyolefin's) for achieving optimum bond strength.

Sensor layout Lines

If required, the position of AFC sensor to be bonded can be marked by a brass needle or a hard 4H-pencil for exact pin pointing of the location.

Adhesive

To have quality bonding of AFC sensors, utmost cleanness is essential. Therefore the bonding is preferably to be made on a dust-free workbench with filtered air supply. For relatively short-term applications in a benign environment, cyanoacrylate (super glue) adhesive (where compatible with the plastic) is often a convenient choice because of the

simple, quick curing procedure. Epoxy adhesives that cure at room temperature or somewhat above the room temperature are eminently suitable for bonding AFC to most types of plastics and composites. These adhesives are available in a wide range of formulations with different characteristics and properties time/temperature/clamping pressure for curing, elongation capability, expected glue line thickness, etc. should be selected accordingly. When necessary for elevated-temperature testing, epoxies which cure or post-cure at higher temperatures can be employed; assuming, of course, that such temperatures are suitable for the plastic or composite.

Pressure

During setting of the adhesive, the AFC sensors have to be clamped with a constant pressure. Spring clamps or C clamps can be used as a universal clamping tool. For economic production and best results of bonding, a specific "tailor-made" clamping tool would be recommended for use to create the pressure. The sensor is covered with a Teflon sheet and a backup plate is placed on top with which helps to apply uniform pressure over the entire AFC sensor

Post Cleaning

After bonding the sensor edges are cleaned of any spills of the super glue. The sensor is checked for the resistance. If the circuit is open then the installation procedure is successful if not then the sensor is closely inspected for location where there is a possibility of short-circuiting of the electrodes.

3.2.5 Poling

Theory

The poling of piezoelectric ceramic fiber in the AFC preform after casting is an important stage in the manufacturing of active fiber composites. Poling is necessary for the activation of piezoelectric properties of the PZT fiber embedded in the epoxy, which is done via the use of an electric field. Figure 3.9 shows the Weiss domains before and after poling.

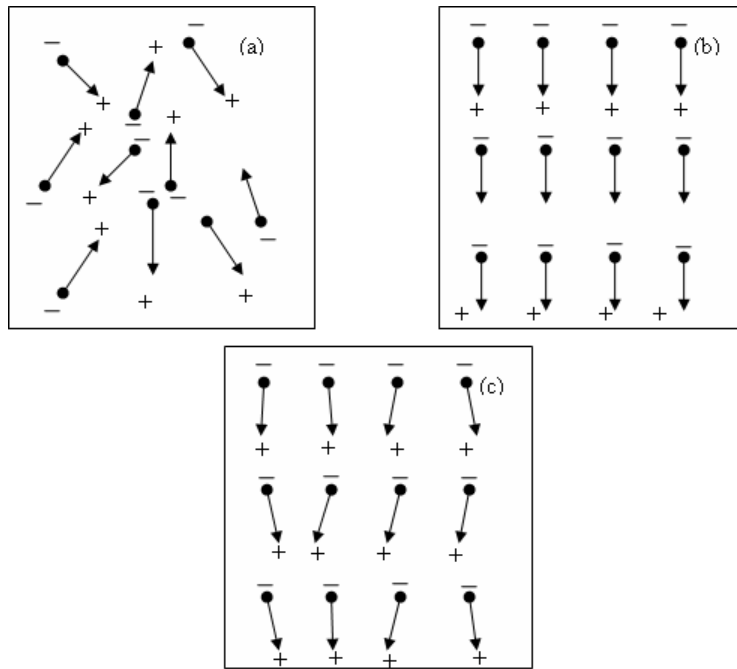


Figure 3.9 Weiss domains; (a) Before poling; (b) During Poling; (c) After Poling

A PZT material consists of electric dipoles which are because of charge separation between the positive and negative ions. Groups of dipoles with parallel orientation are called Weiss domains which can be seen in Figure 3.9. The Weiss domains are randomly oriented in the raw PZT material, before the poling treatment has been finished as seen in Figure 3.9 (a). With the field applied, the material expands along the axis of the field and

contracts perpendicular to that axis as seen in Figure 3.9(b). The electric dipoles align and roughly stay in alignment upon cooling as shown in 3.9(c). The material now has a remnant. When force is applied to a poled piezoelectric material, the Weiss domains migrate proportional to the applied force. The result is a generation of the charge. The various factors that play important role in poling are:

- Poling Temperature
- Electric field

Poling Temperature

The application of a DC voltage at a temperature $T < T_c$ where T_c is the Curie temperature, is limited by ohmic heating due to electronic conductivity, physical breakdown at defects in the ceramic, or by the requirement to allow the migration of space charge within the PZT material. The ideal poling temperature is the curie temperature of the PZT (500° F) however because of limitations on the epoxy matrix; the temperature can't be raised above 180° F.

Electric Field

When an electric field (DC voltage) is applied to a poled piezoelectric material, the Weiss domains increase their alignment proportional to the voltage. The magnitude electric field depends on the temperature at which poling is done. The higher the temperature the lower is the magnitude of the electric field required. An initial poling trial was completed by varying the temperature and the applied field, and then after measuring the response for a lead break the magnitude was finalized. An electric field of 4000V/mm is applied for poling of the AFC sensor.

Poling Procedure

This is the final step in AFC sensor manufacturing. As this involves application of high voltages utmost care must be taken while performing it. The setup consists of a high voltage DC power supply (Glassman High voltage Inc.), a General Electric Countertop Oven and a poling fixture made in house shown in Figure 3.10.

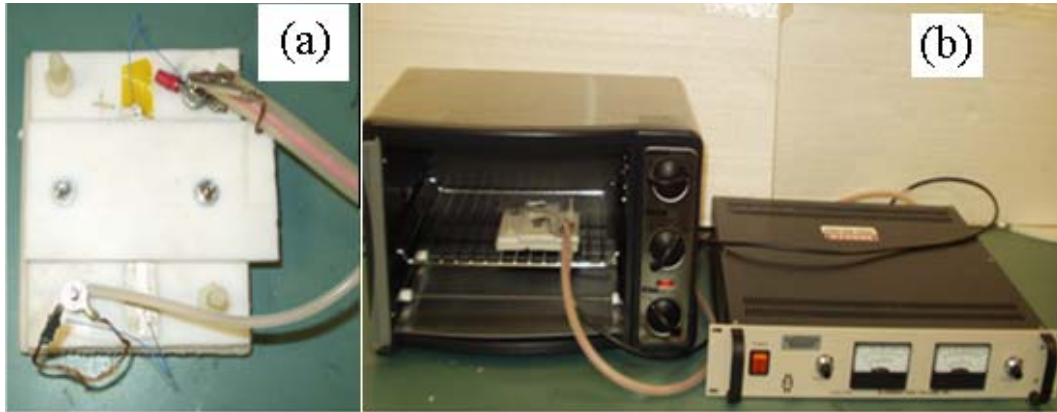


Figure 3.10 Poling setup (a) Poling fixture (b) Entire Poling Setup

The AFC preform is clamped in the fixture. The temperature is set to 180°F on the oven and is closely monitored using a thermocouple. All the connections are made as shown in Figure 3.10

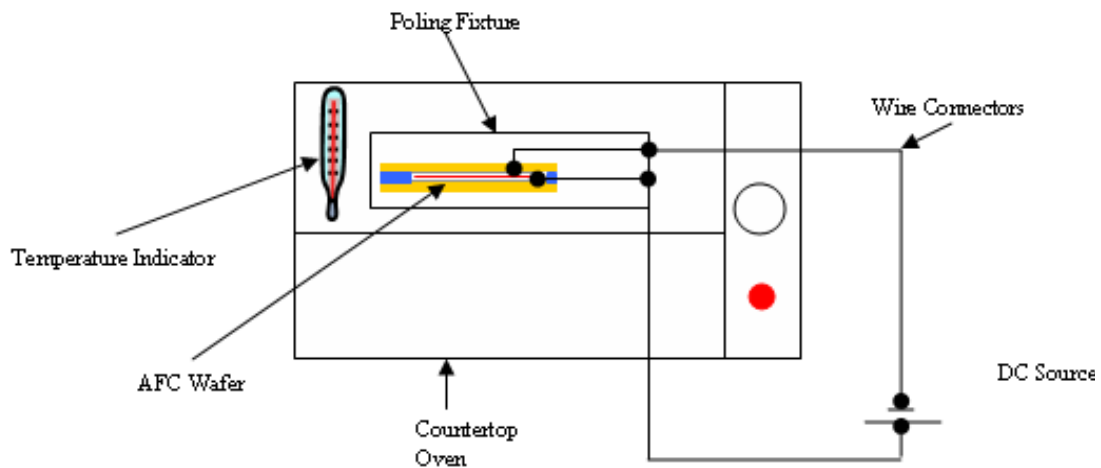


Figure 3.11 Poling Wiring Diagram

Table 3.2 shows the steps in poling along with the time required for each step.

Step No.	Step Detail
1	Clamp the AFC waveform in fixture
2	Make electrical connections as shown in Figure 3.8
3	Start the oven and raise the temperature to 180° F. Soak it for 15 minutes
4	Apply an electric field of 4000V/mm for 10 minutes
5	Turn off the DC supply and take out the fixture from the oven and place it on table
6	Turn on the power supply and apply the same electric field. Use fan for rapid cooling of the fixture to room temperature.
7	Turn off the supply after 15 minutes and remove the electrical connection
8	Check the response of the sensor

Table 3.2 Steps in Poling of AFC sensors

Figure 3.12 shows an AFC sensor manufactured in the Smart Structures and BioNanotechnology lab [4]. Table 3.3 gives the physical dimension of the AFC sensor



Figure 3.12 Manufactured Active Fiber Composite Sensor

Table 3.3 AFC sensor dimensions

Parameter	Value
Length	120.16 mm
Breadth	15mm
Thickness	0.30mm
Weight	36mg

Chapter 4 The Data Acquisition System

The analog and continuous time signals measured by the sensor must be converted into the form a computer can understand. This is what is referred to as data acquisition. Traditionally, measurements are done on stand-alone instruments of various types of instruments like oscilloscopes, multi meters, counters etc. However, the need to record the measurements and process the collected data for visualization has become increasingly important.

There are several ways in which the data can be exchanged between instruments and a computer. Many instruments have a serial port, which can exchange data to and from a computer or another instrument. Use of a GPIB interface board (General purpose Instrumentation Bus) allows instruments to transfer data in a parallel format and gives each instrument an identity among a network of instruments. Another way to measure signals and transfer the data into a computer is by using a Data Acquisition (DAQ) board. A typical commercial DAQ card contains analog to digital converter (ADC) and a digital to analog converter (DAC) that allows input and output of analog and digital signals in addition to digital input/output channels.

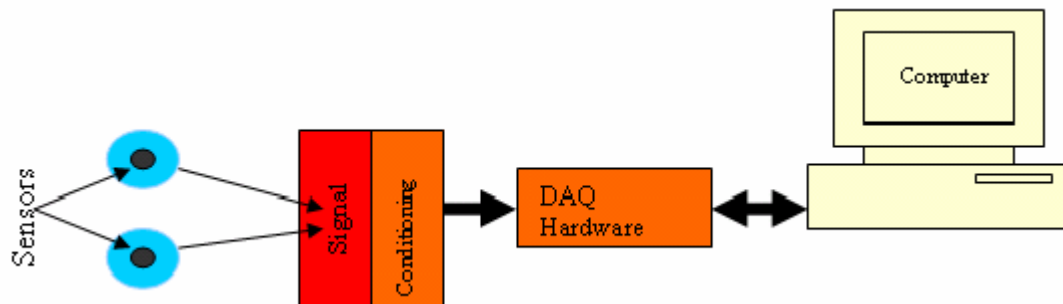


Figure 4.1 Data Acquisition System

The task associated with designing the data acquisition systems are:

- Hardware design
- Software Design
- Testing and Debugging

4.1 Hardware Design

Data acquisition boards and software can be used in a variety of computers. The Basic Analog-to-Digital (A/D) Conversion, Digital-to-Analog (D/A) Conversion and Digital I/O Data acquisition boards help in measuring real-world information represented by analog signals coming from sensors or transducers that convert temperature, pressure, sound, or light into voltage. The electronic sampling of analog signals is called A/D conversion or analog-to-digital conversion. A/D conversion changes real-world analog voltages into digital codes for computer processing and storage. A complementary process, D/A conversion (digital-to-analog conversion) changes digital data into analog voltages. This permits a computer to drive chart recorders, audio amplifiers, process actuators, and other devices requiring an analog driving voltage. Thus DAQ board is the component that listens to the sensors. The choice of DAQ hardware is dependent on various factors including cost.

There are various aspects that are to be considered while choosing a DAQ board.

4.1.1 Signal Type

The type of signal that needs to be acquired namely voltage, current, thermocouple, RTD, thermistor, Frequency voltage, strain gauge etc. The AFC sensor gives out a voltage output. So the signal type was an analog voltage type.

4.1.2 Voltage range

The voltage range depends on the maximum voltage output given out by the SNS box, which was 15V.

4.1.3 Resolution

Precision of the analog input signal converted into digital format is dependent upon the number of bits the ADC uses. The resolution of the converted signal is a function of the number of bits the ADC uses to represent the digital data. The higher the resolution, the higher the number of divisions the voltage range is broken into, and therefore, the smaller the detectable voltage changes. An 8-bit ADC gives 256 levels (2^8) compared to a 12-bit ADC that has 4096 levels (2^{12}). Hence, 12-bit ADC will be able to detect smaller increments of the input signals than an 8-bit ADC. The higher the better.

4.1.4 Number of Input channels

The SNS box gives out two channels of information, which will be expanded into 4 channels later on. So a DAQ board with 4 input channels was selected.

4.1.5 Simultaneous sampling

Simultaneous Sample and Hold (SS&H) systems use a separate sample and hold circuit on each input. When sampling begins, all circuits simultaneously switch to hold, freezing each input signal until it can be sampled by the A/D converter. Multiplexing is to use a single analogue-to-digital converter and switch each signal in turn to the converter. This is a much cheaper solution. However it does not provide simultaneous sampling across the inputs and as more inputs are added the maximum sampling rate is reduced per

input. For example, if a system can read 1 input channel 100 times a second, when reading 10 input channels it is limited to 10 readings per second per channel. Hence a simultaneous sampling DAQ board was selected

4.1.6 Sampling rate

The data is acquired by an ADC using a process called sampling. Sampling analog signal involves taking a sample of the signal at discrete times. This rate at which the signal is sampled is known as sampling frequency. The sampling frequency determines the quality of the analog signal that is converted. Higher sampling frequency achieves better conversion of the analog signals. The minimum sampling frequency required to represent the signal should at least be twice the maximum frequency of the analog signal under test (this is called the Nyquist rate). If the sampling frequency is equal or less than twice the frequency of the input signal, a signal of lower frequency is generated from such a process (Aliasing). The AE signal gives out a frequency of large bandwidth 0-300KHz. So we need a DAQ board with a sampling rate of $2 \times 300\text{KHz} = 600\text{KHz}$ per channel.

Hardware Selection

Data acquisition cards that fit internal PC-computer slots provide cost-effective high-speed multi-channel analogue inputs. A National Instruments simultaneous sampling PCI-6110E was used which have performed impeccably throughout. The 6110E has 4 single-ended analog inputs, suitable for measuring voltages in ranges $\pm 0.05\text{V}$ to $\pm 42\text{V}$. The sampling rate is 1.25Ms/channel with a 12-bit resolution the specifications of which are provided in Appendix D.

4.2 Software Design

DAQ hardware without software is of little use-and without proper controls the hardware can be very difficult to program. The purpose of having appropriate software is the following:

- Acquire, Monitoring and simultaneously processing data in real time
- Controlling the test
- Generating reports in variety of graphical formats
- Stream data to and from disk
- Use various functions of a DAQ board from a single user interface
- Real Time Display
- True Multitasking Operation

4.2.1 Prior Work

There was no previous system in the Smart-Bio-nanotechnology laboratory [4] that was tailor-made for the acquisition and analysis of the AE data. The previous research group used custom programs written in Matlab[®] to run the collect data and analyzed it offline. The user interface and hardware interface routines were all written or accessed using Matlab[®]. No off-the-shelf system exists for these kinds of data acquisition systems, and therefore most research groups develop their own custom software for controlling the lab apparatus.

4.2.2 Limitations of Prior Solutions

The system that was previously used had difficulties regarding limitations of designing highly specialized software for data acquisition using Matlab[®] or C/C++

- They cannot be easily adapted to the requirements of the experiments
- They are not very maintainable It becomes increasingly difficult to maintain and update thousands of lines of program code written using Matlab[®] routines, especially if the original programmer leaves the project.
- It becomes more difficult to add new hardware to the system – One usually needs to rewrite portions of the interface code that accesses the hardware.
- Designing and controlling an experiment often requires a lot of technical savvy, requiring the researcher to write and debug many lines of code, thus detracting.

4.2.3 Problem Statement

The experiment required a software system for conducting monitoring of the structure under fatigue using either PZT patches or AFC sensors. This software system should interface with the data acquisition hardware, provide post-experiment data analysis capability, and be accessible to non-programmers who wish to setup the control flow for the experiments.

4.2.4 Specifications

The specifications for this system can be divided into three broad categories:

1. Data Acquisition
2. Analysis
3. User Interface

Figure 4.2 shows these categories in the form of flowchart

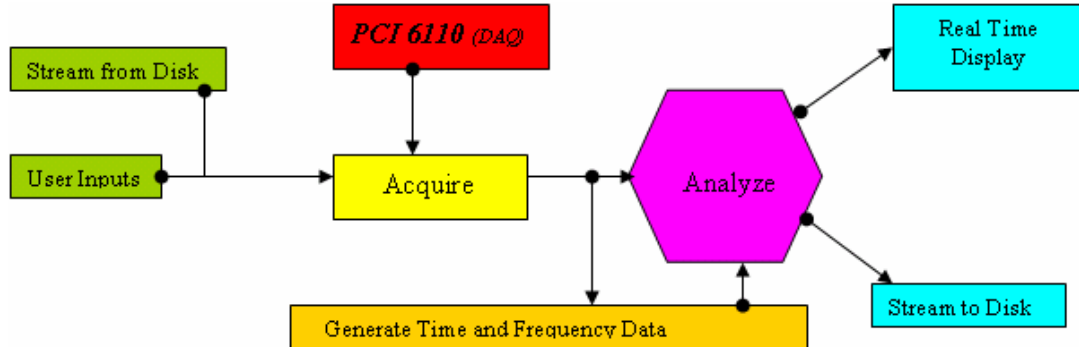


Figure 4.2 Software Requirements

Data acquisition

Each time there is an acoustic emission two analog voltages must be sampled at a minimum of 1MHz. The voltages must be time stamped according to the absolute time. National Instruments data acquisition card available, the PCI-6110e whose specifications include 4 single-ended analog inputs (Please see Appendix D for a data sheet).

Analysis

The data that is acquired must be analyzed in real time. An algorithm is developed which performs the analysis of the acquired signal. Analysis involves:

- Pin pointing which sensor is firing
- Calculating the cumulative peak voltage
- Calculating the cumulative AE hits per sensor
- Calculating the frequency of AE emission

User Interface

- Allow the user to pause or pause an experiment, or cancel it completely, or remove it from further runs while the set of experiments are in progress
- Log the AE data, (crack location and the time information), and also the time of

each acoustic emission

- Allow real-time monitoring of the experiment's status: Show a real-time display of the two channel data against time along with frequency content.
- Once the experiment is over prompt the user to move the logged data from the work directory into the data directory.

Software's under consideration

- Microsoft's Visual C++ environment
- Matlab[®]
- Nation Instruments LabVIEW

The advantages and disadvantages of which are listed in Table 4.1

Table 4.1 Comparison of Various Software Design Environments.

Comparison Characteristic	Matlab [®]	VC++	LabVIEW
Hardware Support	Needs Third Party Drivers	Interface libraries provided	Direct Support
Speed	Slower than VC++ but faster than LabVIEW	Fastest	Slowest
User Interface	Easy, Drag and Drop	Very Complicated	Easy, Drag and Drop
Modular Programming	Possible, with little tweaking	Possible, with little tweaking	Easiest
Learning Curve	Slow	Slow	Fast

LabVIEW was selected as the DAQ software as it not could only do the

\aforementioned tasks in Section 4.2 but also provided flexibility of changing requirements. In addition to this LabVIEW was easier to learn and the development time was short.

In the Figure 4.3 a complete DAQ system with LabVIEW is shown. The driver software is a lower level driver that interfaces LabVIEW software with the DAQ boards. As a user of LabVIEW one does not have to worry about configuration and control of components within DAQ boards. LabVIEW identifies each board by a device number and therefore one can have as many devices as the computer can accept on their expansion slots. LabVIEW can also combine and display inputs from various sources like inputs from serial and parallel port, DAQ boards, and GPIB boards on a single interface as shown in Figure 4.3.

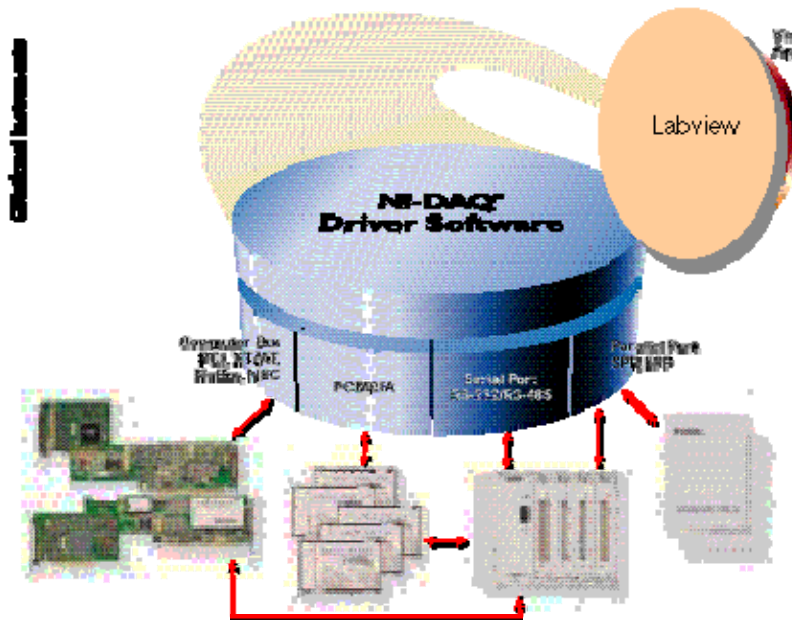


Figure 4.3 LabVIEW Software and DAQ system [ref www.ni.com]

LabVIEW is programmed with set of icons that represents controls and functions, available in the menu of the software. Such a programming is called visual programming

and National Instruments calls it G. The user interface, which is called a VI consists of two parts- a front panel and a diagram. This is similar to that of an instrument where a front panel is used for an input, output controls, and to display the data whereas the circuit resides on the circuit board. Similarly you can bring the buttons, indicators and graphing and display functions on the front panel as LabVIEW is used to perform system simulations, since it contains many commonly used filter, digital signal processing, and statistical functions. LabVIEW compiles almost as fast as C or Matlab[®].

While developing the graphical interface the data acquisition and analysis was done in real time along with the real time display. Before the actual programming the tasks were simplified into a flowchart and then the coding was done. This reduced the development time and also ensured that the seamless integration of all the requirements was done.

4.2.5 Development of the LabVIEW system

The following block diagram gives an analogous representation of how the Virtual Instrument (VI) works. The LabVIEW Front panel consists of all the controls and the indicators while the wiring diagram is in the block diagram (Appendix A). Before implementing the algorithm the parameters that needed to be monitored along with the required outputs were individually programmed. The Entire shm.vi is made up of different SubVI which can be seen in Table 4.2

Table 4.2 Sub VI's in shm.vi

Sr No	Name of VI	Process description
1	input.vi	This SubVI includes two sections: one reads the data from a text file that is stored. The second one provides friend user interface for user to adjust the parameters like threshold voltage, peak detection voltage
2	daq.vi	This SubVI does the actual interfacing with the PCI 6110e and generates the waveform data from two channels for further analysis
3	time.vi	This SubVI generates the time and frequency data necessary for further analysis
4	peak.vi	The function of this SubVI is to calculate the no of AE hits on each sensor and the cumulative voltage
5	output.vi	Used to plot the raw data , analyzed data and streaming to disk
6	shm.vi	This GUI incorporates all the above SubVI viz setup, acquisition analysis and output

The data was in the form of two channels form the SNS box as shown in Table 4.3 and Figure 4.4

Table 4.3 Number of Channels

Channel Number	Type of Information
Channel 0	Crack Location
Channel 1	Time information

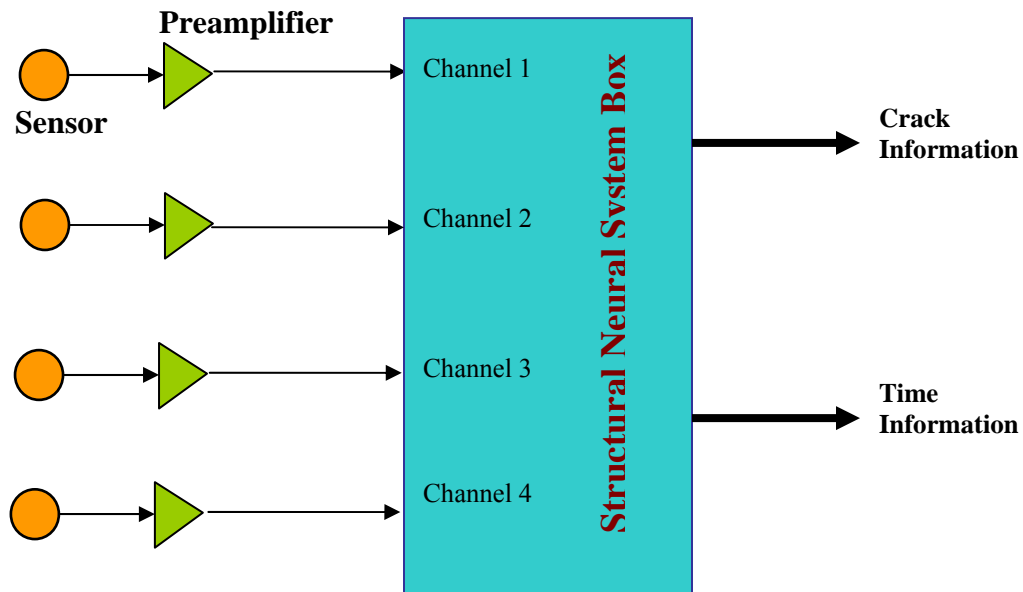


Figure 4.3 Sensing architecture

The main constraint on this was the frequency at which the data needed to be sampled which was dependant on the frequency content of the data. Typically, AE systems operate in a range of 1 kHz to 2 MHz or greater in frequency. The lower frequency limit is imposed by background noises such as friction, outside impacts, or process generated signals, that tend to mask acoustic emissions. The upper frequency limit is imposed by attenuation, which tends to limit the range of detection of acoustic emission signals. A critical part of the AE application process is the selection of a suitable frequency range for AE detection and signal processing. It must be above the non-AE related background noises, while providing the necessary detection range (distance/frequency) and sensitivity to AE related signals. Hence the sampling frequency was set at 1MHz which was the limited by the bus bandwidth speed of the computer.

4.3 Testing and Debugging

Various debugging techniques where used in LabVIEW

4.3.1 Finding Errors

Click the broken Run button or select Windows>>Show Error List to display the Error list window, which lists all the errors. Double-click an error description to display the relevant block diagram or front panel and highlight the object that contains the error

4.3.2 Execution Highlighting

Execution highlighting shows the flow of data on the block diagram from one node to another using a bubble that move along the wires. Use execution highlighting in conjunction with single stepping to see how data move from node to node through a VI.

4.3.3 Single-Stepping

Single-step through a VI to view each action of the VI on the block diagram as the VI runs. The single-stepping buttons affect execution only in a VI or subVI in single-step mode. Enter single-step mode by clicking the Step over or Step into button.

4.3.4 Probes

The Probe tool is used to check intermediate values on a wire as a VFI runs. When execution pauses at a node because of single stepping or a breakpoint, the wire can be probed after it has executed to see the value that flowed through that wire.

A custom probe can be created to specify which indicator to view the probed data. For example, for viewing numeric data, a chart within the probe can be used to see that data.

4.3.5 Breakpoints

Breakpoint tool can be used to place a breakpoint on a VI, node, or wire on the block diagram and pause execution at that location. After setting a breakpoint on a wire, execution pauses after data pass through the wire. A breakpoint can be placed on the block diagram workspace to pause execution after all nodes on the block diagram execute.

When a VI pauses at a breakpoint, LabVIEW brings the block diagram to the front and uses a marquee to highlight the node or wire that contains the breakpoint. LabVIEW highlights breakpoints with red borders for nodes and block diagrams and red bullets for wires.

4.3.5.1.1 Testing

The developed system was run using signal generators (Agilent function generator) to simulate the AE signal. The data acquisition performed according to specifications up to a sine frequency of 1MHz before it started dropping samples (much higher than the maximum of 1MHz required). With the known input the output was measured and the system logic was verified. Figure 4.5 shows the front panel or the graphical user interface of the shm.vi that was built using LabVIEW. The VI monitors the AE data from the neurons continuously. The trigger level in the neurons is set depending upon the material under fatigue testing. Whenever an AE occurs, the number of acoustic events on neuron-1 and neuron-2 are recorded by the VI and are counted and then plotted against the number of stress cycles that the structure undergoes. The number of stress cycles can be determined by a separate PZT sensor on the structure. In addition, the peak voltages are measured for each AE and are plotted against the number of cycles. The data generated is stored in a spreadsheet for further analysis. The VI uses visual and sound indicators to alert the operator each time an AE occurs.

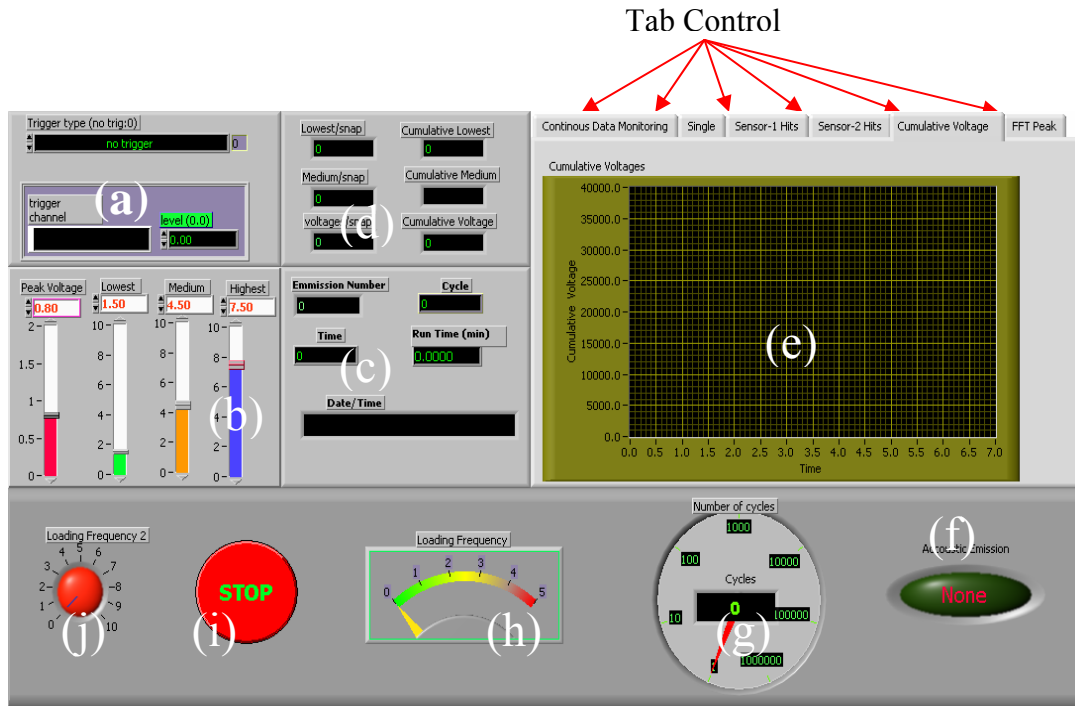


Figure 4.4 LabVIEW front panel layout a) Trigger parameters; (b) analysis parameters (c) date and total running time and number of stress cycles; (d) firing neurons and LP filtered cumulative AE voltage; (e) displayed parameter depending on the tab control; (f) LED indicator showing AE; (g) number of stress cycles; (h) frequency of vibration (i) Stop button to stop execution of the Virtual Instrument; (j) Loading frequency

Chapter 5 Experimentation

5.1 Testing the SNS on a Riveted Aluminum Plate using Lead Breaks

Riveted aluminum structures are used extensively in aerospace structures. To monitor them effectively and continuously, a large number of sensors are required to detect crack growth. To study the possibility of the use of the SNS on riveted structures, an aluminum riveted plate (Figure 5.1) was constructed and was tested to see if the SNS can locate the simulated AE. This plate was constructed of three aluminum plates (7075 – T6) joined with rivets as shown in Figure 5.1. Figure 5.1(a) shows the aluminum riveted plate. Figure 5.1(b) shows the geometric modeling of the plate along with the placement of PZT sensors. Two of the base plates have dimensions 15.29 X 15.29 X 0.305 (cm). The plate used to join the bottom two plates has dimensions 15.29 X 0.762 X 0.305 (cm). The plate was joined using 12 rivets. A Lead Zirconium Titanate (PZT) single sheet was purchased from Piezo Systems Inc. to form the individual sensor elements. The material was PSI – 5A 4E with dimensions 7.24 X 7.24 X 0.027 (cm). This sheet was cut manually using a sharp razor blade to 1.524 X 0.889 X 0.00267 (cm) dimensions. Five monolithic PZT's were made. These PZT's were bonded onto the aluminum plate using superglue. Kapton[®] was used as an insulating layer between the PZT and the aluminum plate. Since the current SNS prototype had only a 2 sensor input capability, sensors 2 and 4 (shown in Figure 5.1(b)) were used to predict the location of the AE. For the first case an AE was generated using a pencil lead break near sensor 4. For the second case an AE was generated near sensor 2.

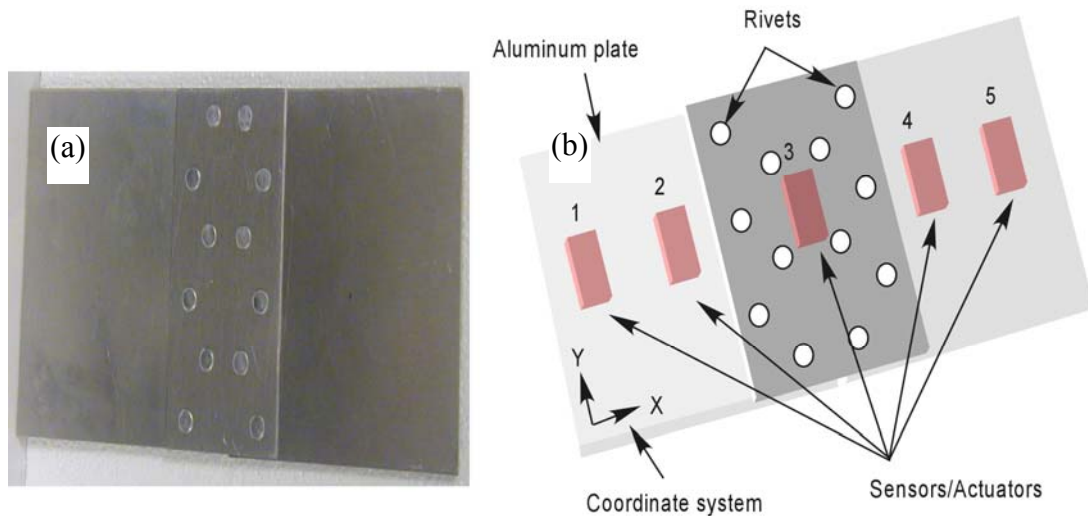


Figure 5.1 Aluminum Rivet Plate; (a) Picture of the plate, (b) Geometric model of the riveted plate along with sensors

The riveted aluminum plate was loaded using a Mechanical Testing Systems (MTS) machine. For the current paper the response of the SNS for fatigue failure due to bending has not been shown. The set-up of the MTS machine is shown in Figure 5.7 Using a four point bending fixture the aluminum riveted plate was excited with an input frequency of 3 Hz. The SNS analog processor box had sensors 2 and 4 as inputs which is developed in Smart Structures and BioNanotechnology [4] by Mr. Goutham Kirikera. Table 5.1 shows the pre-assigned voltage values that have been assigned for different neurons. Sensor 2 was pre-assigned a DC voltage of 3/0 volts (ON/OFF state) and sensor 4 was pre-assigned with a DC value of 5/0 volts (ON/OFF state). The reference voltage of the SNS analog processor box was set at +3 volts. The response of the SNS analog processor box is shown in Figures 5.2 and 5.3. For a better understanding the geometric model, the riveted plate is placed on the top of Figures 5.2 and 5.3

Table 5.1 Pre-Assigned Voltages for Different Neurons.

Neurons Firing	Pre-assigned voltages		SNS response (Volts)
	Sensor 2 (Volts)	Sensor 4 (Volts)	
None	0	0	0
Sensor 2	3	0	3
Sensor 4	0	5	5
Sensor 2 and Sensor 4	3	5	8

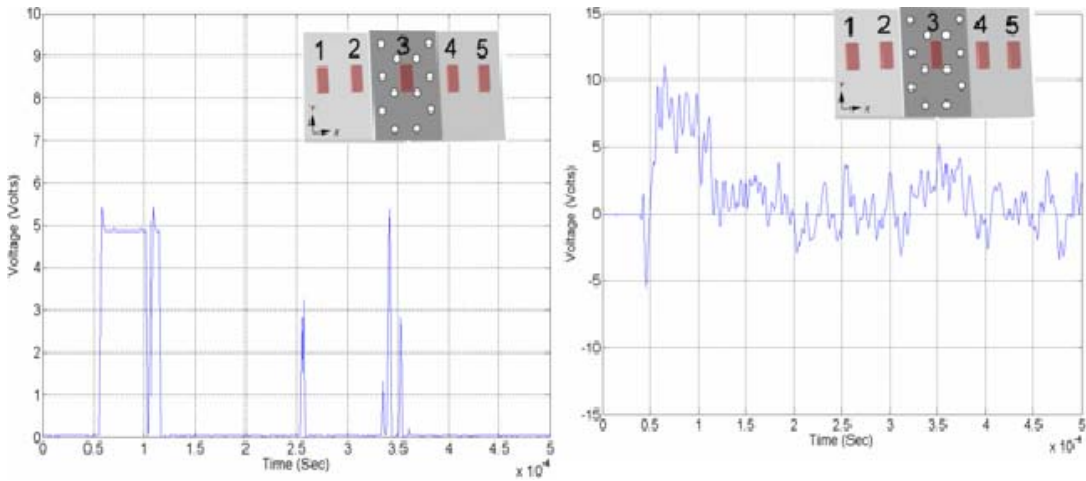


Figure 5.2 Response of SNS for an AE lead break located near Sensor 4; (a) Crack information, (b) Time waveform of the cumulative AE

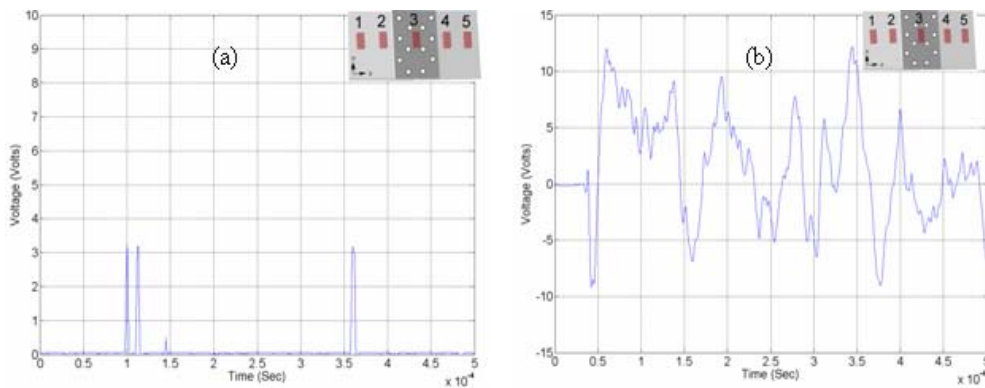


Figure 5.3 Response of SNS for an AE lead break located near sensor 2; a) Crack information, b) Time waveform of the AE

Figure 5.2(a) shows the initial amplitude of 5 volts indicating that the AE was located close to sensor 4. The firing of 3 volts in Figure 5.2(a) that follows the initial 5 volt peak indicates that sensor 2 has also detected the waves that are propagating in the structure. Figure 5.2(b) shows the time domain waveform of the response of the plate due to a simulated AE (pencil lead break) indicating the high frequency content of the waveform. Similarly Figure 5.3 shows the response of the SNS analog processor box for an AE whose source was located close to sensor 2. The initial amplitude of 3 volts in Figure 17(a) indicates that the AE was located near sensor 2. Figure 5.3(b) shows the cumulative time domain voltage information of the straining of both the sensors. The initial peak in time domain waveforms is used to interpret the frequency content of the AE. Note that even though the sensor is being excited by the excitation frequency of the MTS machine the SNS analog processor box automatically filters out the low frequency data and outputs only the data from the high frequency AE.

5.2 Capacitance effect of the sensor

A PZT acts as a capacitor that has charge attraction/repulsion due to strain. When using a PZT as a sensor or actuator on an aluminum structure, it is possible that the structure can serve as the ground or return circuit for the PZT by bonding the PZT directly to the electrically conductive structure. However, this approach will have current flowing in the structure to the PZT electrodes, and the PZT can generate 200 volts or more due to an impact to the structure or when driven to generate waves for active damage interrogation. If the ground circuit became degraded or interrupted due to corrosion or loosening, the sensor signal may become degraded and there could be arcing in the connection that in some situations might be dangerous. Also, if the aluminum were

to become live due to a lightning strike or through faults in the vehicle electrical system, the sensor system would possibly be damaged. Therefore, here the PZT is encapsulated in a Kapton[®] film that has a large electrical resistance that will prevent any current flow through the film. A thin Kapton[®] film is used to minimize shear lag that will reduce the strain in the PZT. It was found that the layer consisting of the Kapton[®] sheet and the glue between the aluminum plate and PZT acted as a capacitor and can cause small currents to flow in the structure. The impedance of this capacitor was calculated by using a simple impedance measurement circuit. Figure 5.4(a) shows the impedance measurement circuit that was used to calculate the capacitance of the Kapton[®] film and the bond layer. In the circuit the top electrode of the PZT sensor was not connected. This is because our primary interest is in measuring the capacitance value and impedance only of the bond layer. The thickness of the superglue and Kapton[®] sheet has been exaggerated for clarity in Figure 5.4(a). The resistors R1 and R0 refer to a known resistance of 10K Ω used for testing, and an oscilloscope resistance of 1M Ω , respectively. Figure 5.4(b) shows the variation of impedance of the bond layer as a function of frequency. The capacitance of the PZT sensor was measured using a capacitance meter and was found to be roughly 8 μ F. The average capacitance of the bond layer was found to be in the order of 0.3 nF. The infinite impedance at low frequencies shown in Figure 5.4(b) is due to the high resistance of the Kapton[®] layer.

An interesting result of studying the capacitive effect of multiple PZT sensors that are bonded to the aluminum and individually electrically insulated and connected to separate channels of an oscilloscope is that if the aluminum plate is not grounded, the electrical signal from one PZT due to strain is received at all the others immediately and this can

obscure the later signal due to the acoustic waves traveling to the other sensors. The plate structure and the Kapton[®] film and the bottom electrode of the PZT form a capacitor and may cause very small currents to flow in the ground circuit. In practice, the operation of the neural system generates sensor voltages at high frequency less than one volt, and the power is very low. The capacitive coupling to the structure is only at high frequency and produces a very small current.

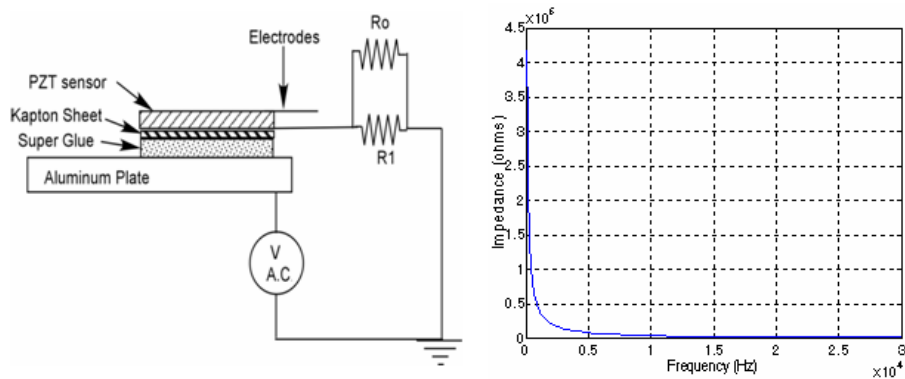


Figure 5.4 Measurement of Impedance of the Kapton[®] and superglue layer (a) Impedance measurement circuit, (b) Variation of Impedance with frequency

5.3 Pulse Excitation

The riveted aluminum plate was tested for propagation of AE with the aid of pulse excitation. This would tend to produce flexural waves in the plate. Figure 5.6(a) shows the excitation voltage used to excite the actuators embedded on the aluminum plate. The excitation voltage applied from the signal generator to the amplifier was a rectangular pulse. Because of the limited bandwidth of the amplifier, the signal shape has been distorted. Figures 5.6(b) and 5.7 show the response signals obtained from the PZT's attached to the structure. In Figures 5.5 and 5.6 in the legend, 'A' refers to the PZT that is being used as an actuator. Similarly 'R' refers to the response of the corresponding sensors. The geometrical location of PZTs on the riveted plate is shown on the top left of

each Figure. It can be seen from Figure 5.5(b) that the amplitude of the response of the sensors decreases as the waves propagate through the thick section of the lap joint. The amplitude of strain in the thick section is much less than in the thin section. This is expected because of the displacement being inversely proportional to the bending inertia. Figure 5.6(a) shows the response of sensors 2 and 4 for an excitation produced on the structure using PZT 3. It can be seen that most of the high frequency waves get damped out or are reflected due to travel from thicker section to thinner section. Figure 5.8(b) shows the response of sensors 2 and 3 for an excitation produced using PZT 5. It could be inferred from all the three graphs that most of the high frequency waves get reduced in amplitude when traveling from one section of the plate to the other section.

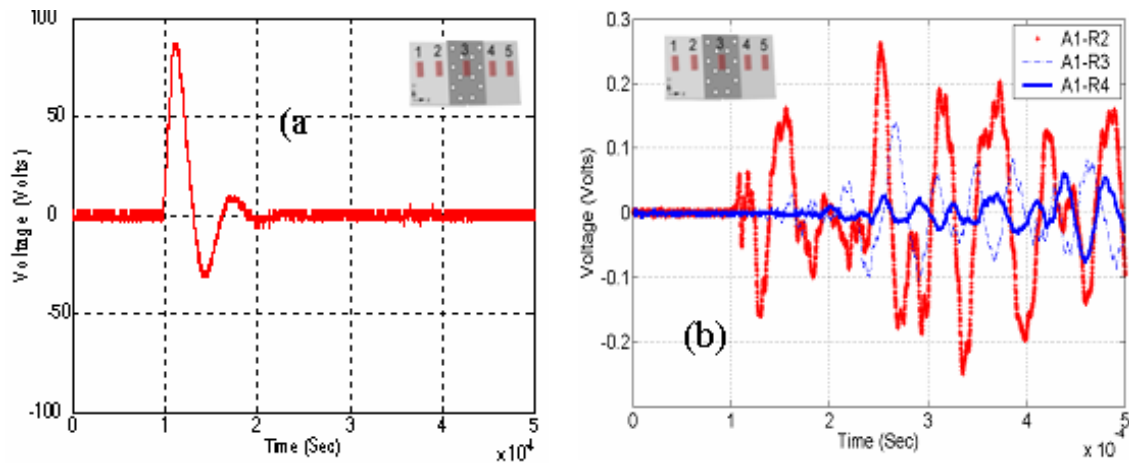


Figure 5.5 Excitation to the PZT; (a) Pulse Excitation, (b) Response of sensors 2, 3 and 4 for a pulse excitation to PZT-1

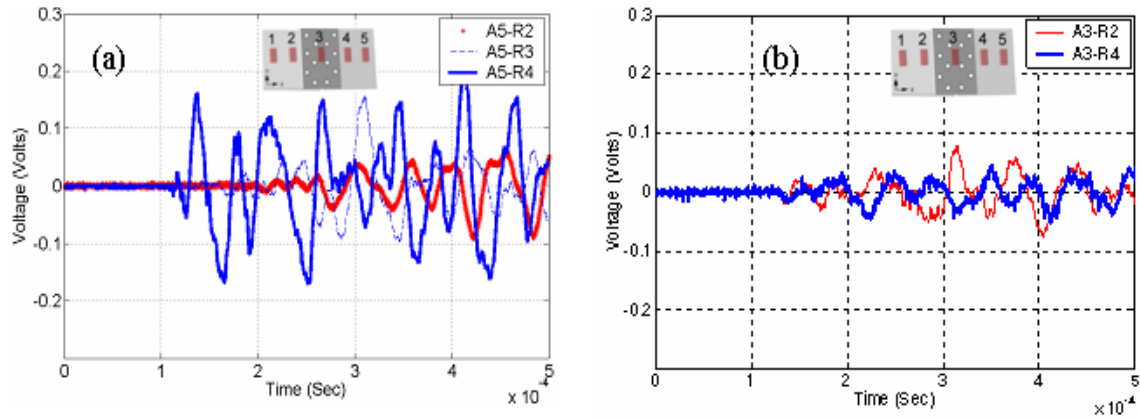


Figure 5.6 Actuation through the joint; (a) Response of sensors 2 and 4 for an excitation with PZT 3; (b) Response of sensors 2, 3 and 4 for a pulse excitation from PZT-5

5.4 Dynamic Testing of an aluminum plate

The study of propagation of AE through an aluminum plate was done using three experimental setups. The first consisted of loading the riveted aluminum plate joint on the MTS machine by applying a bending load. AE was provided by manually breaking a pencil lead on the surface and the location was determined using the SNS analog processor. To further investigate that the SNS analog processor can detect the original AE produced by the development of cracks, a second experimental setup was designed by providing a notch on a narrow aluminum plate and loading it (bending load) in the MTS machine to produce a crack. The third experiment did not use the SNS and was to study AE in aluminum plates using conventional AE sensors and applying a tension load using a larger MTS machine.

5.5 Fatigue Testing of a Riveted Aluminum Joint

The riveted aluminum plate previously tested for pulse excitation was further tested on an MTS machine. Figure 5.6 shows the setup of the riveted aluminum plate mounted on a MTS machine and fatigue loaded. An input of 3 Hz was provided to the aluminum plate

joint. Sensors 2 and 4 (shown in Figure 5.1) were connected to the SNS analog processor box to verify if the SNS box does indeed predict the location of the acoustic emission.



Figure 5.7 Setup of MTS machine and LabVIEW data acquisition system to test the riveted aluminum plate

With the plate being fatigue loaded, an acoustic emission was provided manually using a pencil lead break near sensor 4. The SNS electronic box had sensors 2 and 4 as inputs. Sensor 2 was pre-assigned a DC voltage of 3 volts and sensor 4 was pre-assigned with a DC value of 5 volts. The reference voltage of the SNS analog processor box was set at 3 volts. With the plate being fatigue loaded and an acoustic emission manually provided near sensor 4, the response of the SNS analog processor is shown in Figures 5.8 and 5.9. Figure 5.8(a) shows the initial amplitude of 5 volts indicating that the acoustic emission was located close to sensor 4. The firing of 3 volts shown in Figure 5.8(a) indicates that sensor 2 has also detected the AE. Figure 5.8(b) shows the time domain waveform of the simulated AE indicating the high frequency content of the waveform. Similarly Figure 5.9 shows the response of the SNS for an excitation located near sensor 2. The initial amplitude of 3 volts in Figure 5.9(a) indicates that the AE was located near sensor 2. Figure 5.9(b) indicates the time domain information of the straining of both the

sensors. The initial peak in time domain waveforms indicates the frequency content of the AE. Note that even though the sensor is being excited by the excitation frequency of the MTS machine, the SNS analog processor automatically filters the low frequency data and outputs only the high frequency acoustic emission and no fretting or noise interference of the MTS occurred. The joint is being used for sensor design studies and later joint sections will be tested to fatigue failure with the SNS attached.

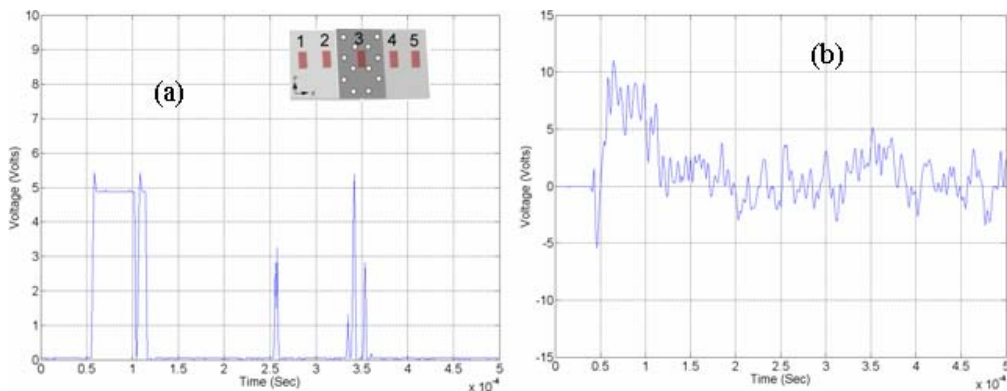


Figure 5.8 Response of SNS for an AE lead break located near sensor 4, (a) Crack Information, and (b) Time waveform of AE

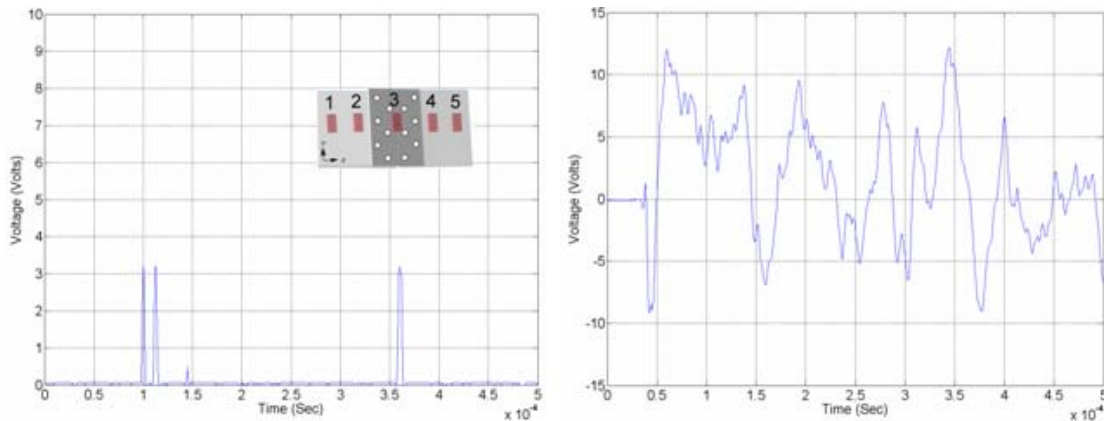


Figure 5.9 Response of SNS for an AE lead break located near sensor 2, a) Crack Information b) Time waveform of AE

This testing indicates that the neuron of the SNS should be placed in the section of the structure where the AE occurs and that it is difficult to detect the AE wave after it travels in a joint from a section of one thickness to a section of another thickness. This is a

preliminary conclusion as testing in which the joint is fatigued and testing using long neuron sensors is needed.

5.6 Monitoring AE on an Aluminum Plate using the SNS

The previous section showed that SNS analog processor can predict the location of simulated AE with only one channel of data acquisition. This architecture will be extended to have many simultaneous neurons. The SNS analog processor was next tested in a simulated real time environment. Figure 5.10 shows the geometry of a 7075-T651 aluminum plate with a notch provided at the center span and side of the plate. The yield strength for this material as specified by the manufacturer is 73ksi. A thin aluminum plate was subjected to four point bending in an MTS testing machine. P_a and P_b are the loads applied from the MTS machine while R_a and R_b are the reactions from the supports. Two sensors were bonded to the aluminum plate using superglue. The narrow aluminum plate had 12" X 2.48" X 0.19" dimensions.

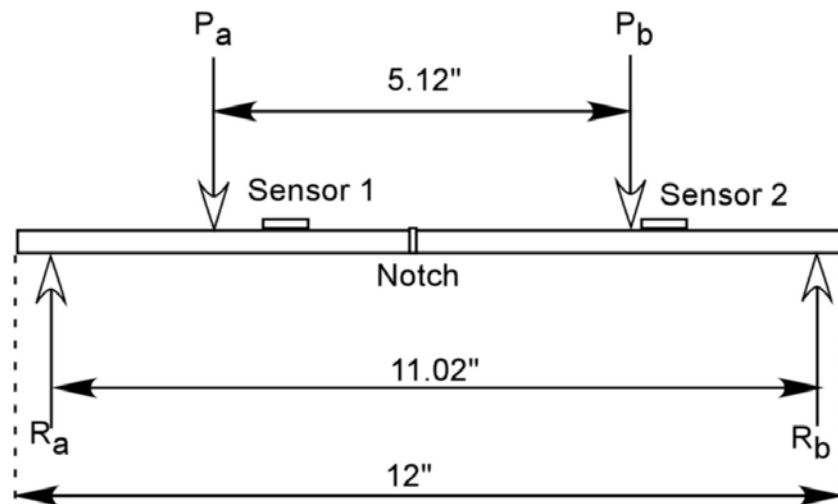


Figure 5.10 Geometry of a narrow aluminum plate with supports

Figure 5.11 shows the crack that was generated due to the cyclic loading of the aluminum plate. In Figure 5.11 the starter notch is shown. Due to a high stress concentration near

the notch, the crack starts progressing in the plate releasing strain energy due to bending of the plate. The plate in Figure 5.11 is straight and exhibited final brittle fracture without gross yielding.

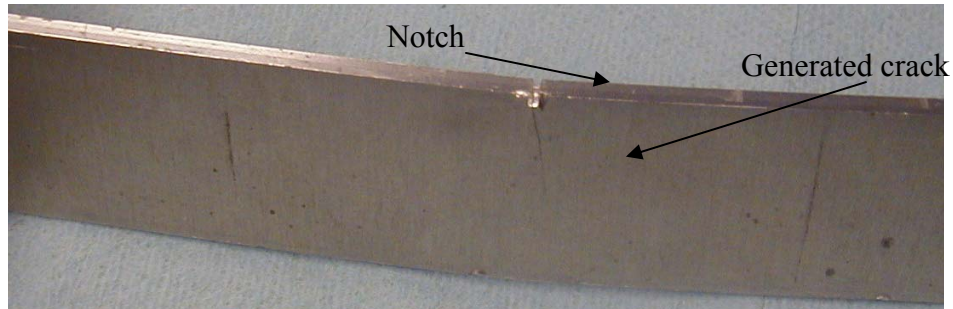


Figure 5.11 Crack generated due to loading the aluminum plate on the MTS machine (the plate is straight and finally fractured without bending)

In a similar set-up to the riveted aluminum joint test, sensor 1 was provided with a constant DC voltage of 3 volts and Sensor 2 was provided with a constant DC voltage of 5 volts. A reference voltage of 0.75 volts was set for each sensor. Whenever each sensor response crosses 0.75 volts the SNS responds by firing the DC voltage corresponding to those sensors. Figure 5.12 shows the response of the SNS analog processor. Figure 5.12(a) shows that the crack is located close to sensor 1. The repeated firing seen in Figure 5.12(a) is due to the reflection of waves from the boundaries. It could be noticed that the firing voltage of sensor 1 is not constant as predicted. This is because of the low bandwidth of the components and the low response time of the components used in the SNS analog processor box, which was designed for monitoring a composite material. The high frequency does not give enough time for the components in the SNS analog processor to fire the required voltage of 3 volts. Figure 5.12(b) shows the response of SNS analog processor box indicating the high frequency AE due to crack propagation in the structure. It was initially surprising to see that there was no response of Sensor 2

through the SNS analog processor. It was later found that sensor 2 was placed beside the loading point of the MTS shown as P_b in Figure 5.10, and most of the high frequency AE is damped when passing through the load point. For a few cases of AE due to crack growth that are not shown, there was a response from sensor 2 also. During these cases the amplitude of AE was large indicating a very large release of energy. In the beginning the AE levels were small and infrequent. As the crack grew the frequency of the bursts and the amplitude increased and the AE signal near failure was clipped during data acquisition.

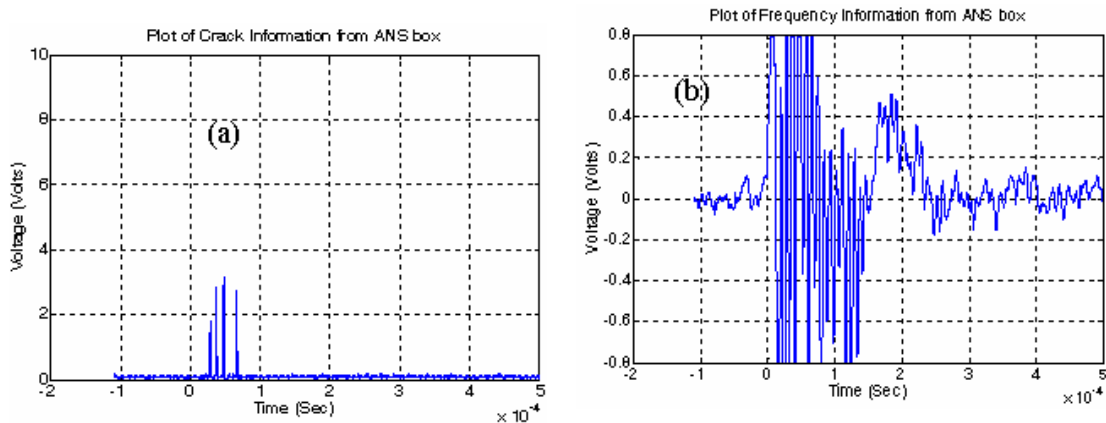


Figure 5.12 Response of SNS analog processor; (a) Crack Location Information, and (b) Time domain waveform

This test showed that the SNS can detect AE if the sensor is close to the damage. Also, two different width sensors were tested. The wider sensor gave a larger voltage output but cut-off some of the high frequency signal. The narrower sensor captured the higher frequency signal, but the amplitude was lower partly due to the smaller area of the sensor. This sensor experiment indicates that a long narrow sensor is needed.

Chapter 6 Sensor Characterization

In this chapter experiments are performed to characterize the properties of the AFS. The beam is cut out from a larger fiber glass sheet in the machine shop. The dimensions of the beam are listed below

- Length of beam 0.254 m.
- Width of beam 144.6 mm.
- Thickness of beam 6.175 mm. Figure 6.1 shows the three AFC sensors which are bonded on the Fiber glass plate.

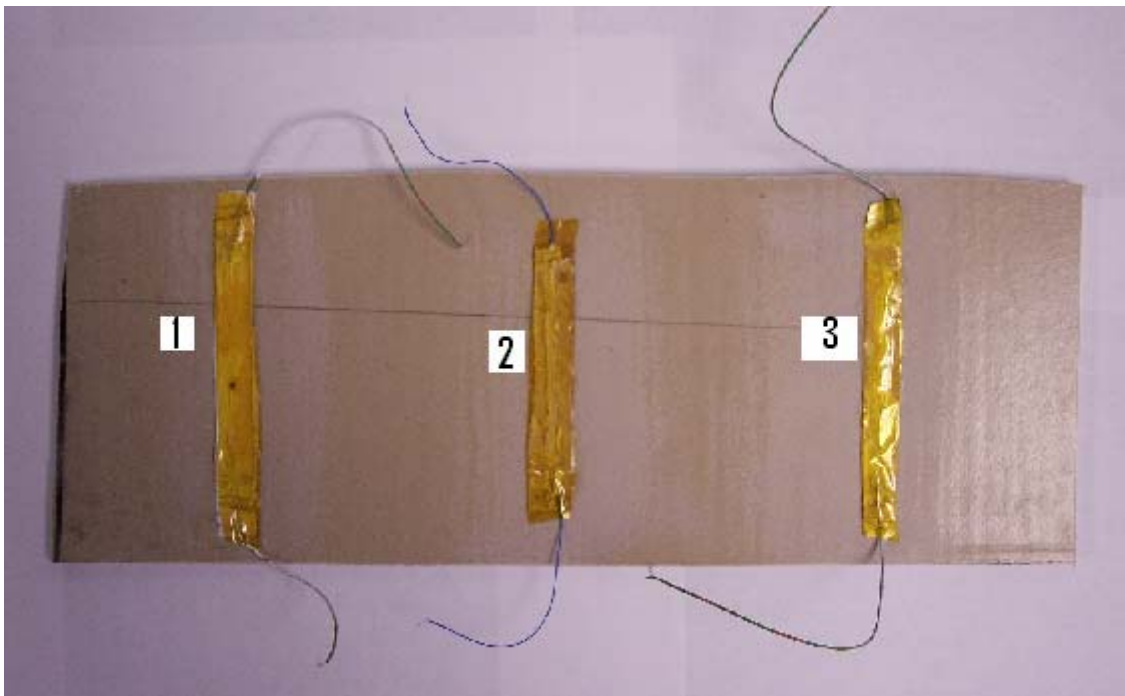


Figure 6.1 Fiber glass plate size with three bonded Active fiber composite sensors

The beam with the bonded sensors is simply supported on two wooden supports as shown in Figure 6.2. The sensors were bonded using super glue on the pate.

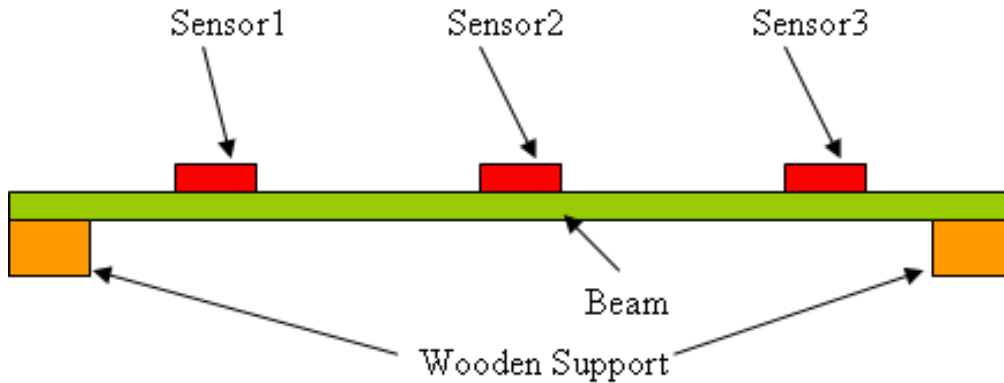


Figure 6.2 Simply supported beam

Testing of beam with the AFC sensors is done for:

- Low frequency
- High frequency (Lead break)
- Sensors in series
- Sensors in parallel
- AFC actuation
- Power harvesting.

6.1 Low frequency response of the sensor

For testing the low frequency response of the sensor, a light tap was given to the beam at three different locations, i.e. near each sensor. The responses generated by the three sensors were captured using 3 separate channels of the Tektronix Oscilloscope. The results are shown in the following Figures 6.3, 6.4, 6.5. Figure 6.3 shows the response for a low frequency tap near sensor1, Figure 6.4 shows the response for a low frequency tap near sensor1, and Figure 6.5 shows the response for a low frequency tap near sensor-1.

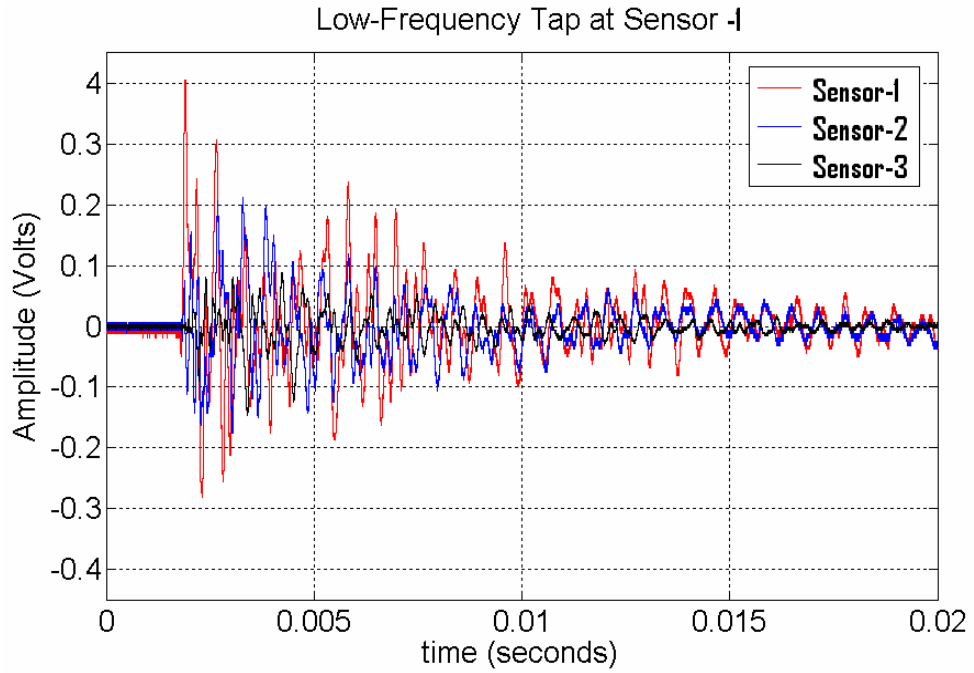


Figure 6.3 Response of sensor-1, 2, 3 for low frequency tap at sensor-1

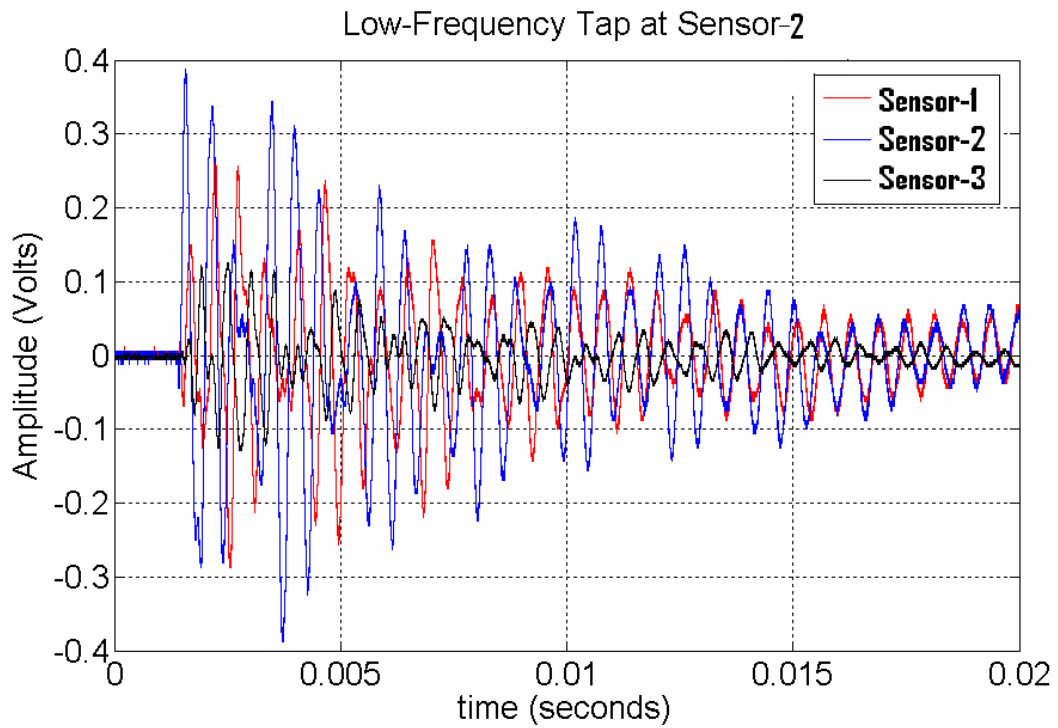


Figure 6.4 Response of sensor-1, 2,3 for low frequency tap at sensor-2

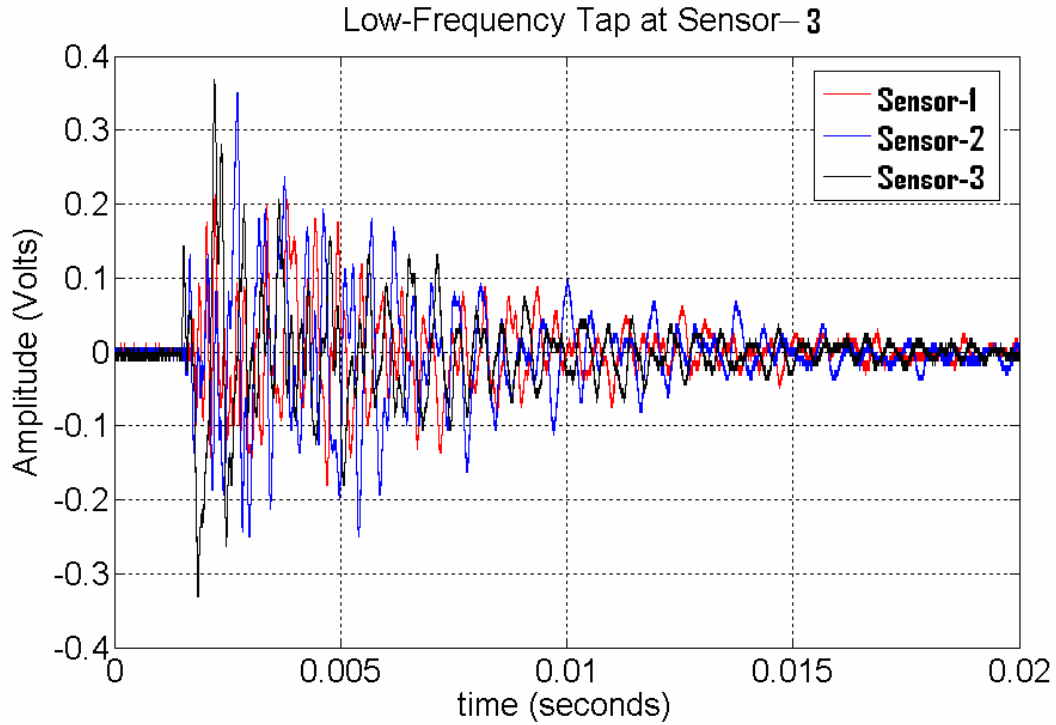


Figure 6.5 Response of sensor-1, 2, 3 for low frequency tap at sensor-3

Figures 6.3, 6.4, 6.5 show that the sensors can pick up low frequencies. It can be seen in Figure 6.3 that sensor-1 has the highest amplitude followed by sensor 2 and 3. In Figure 6.4, sensor-2 has the highest amplitude, while sensors 1 and 3 have almost same response but less than sensor-2. In Figure 6.5 the response of sensor-3 is the highest followed by sensor 2 and 1. From Figures 6.3, 6.4 and 6.5 it can be inferred that the amplitude of the response of the sensors decreases as the waves travel away from the source because of damping.

6.2 High frequency response of the sensor (Lead Break)

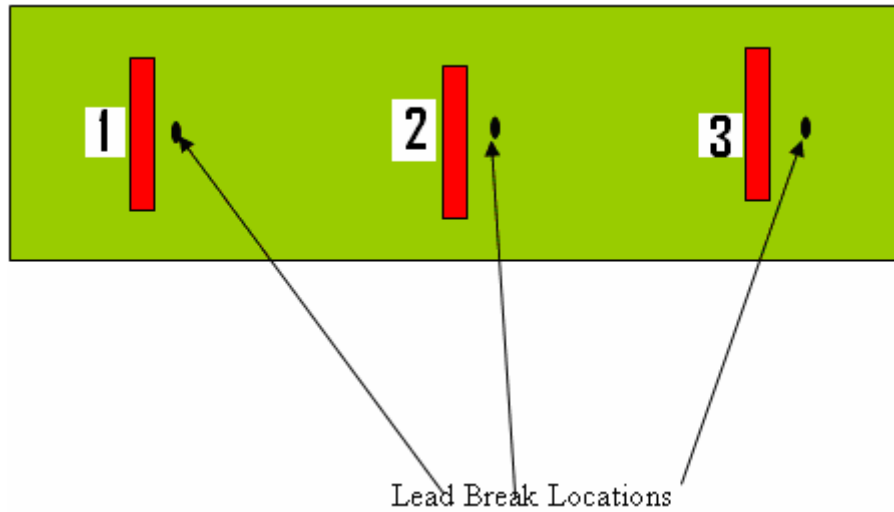


Figure 6.6. Lead break location on the beam plate

Using the same set-up 0.5mm pencil lead breaks were done near the center of each sensor as shown in Figure 6.6 and the response was filtered using a bandwidth Kron-hite filter between 30KHz – 500KHz with a 40dB gain.

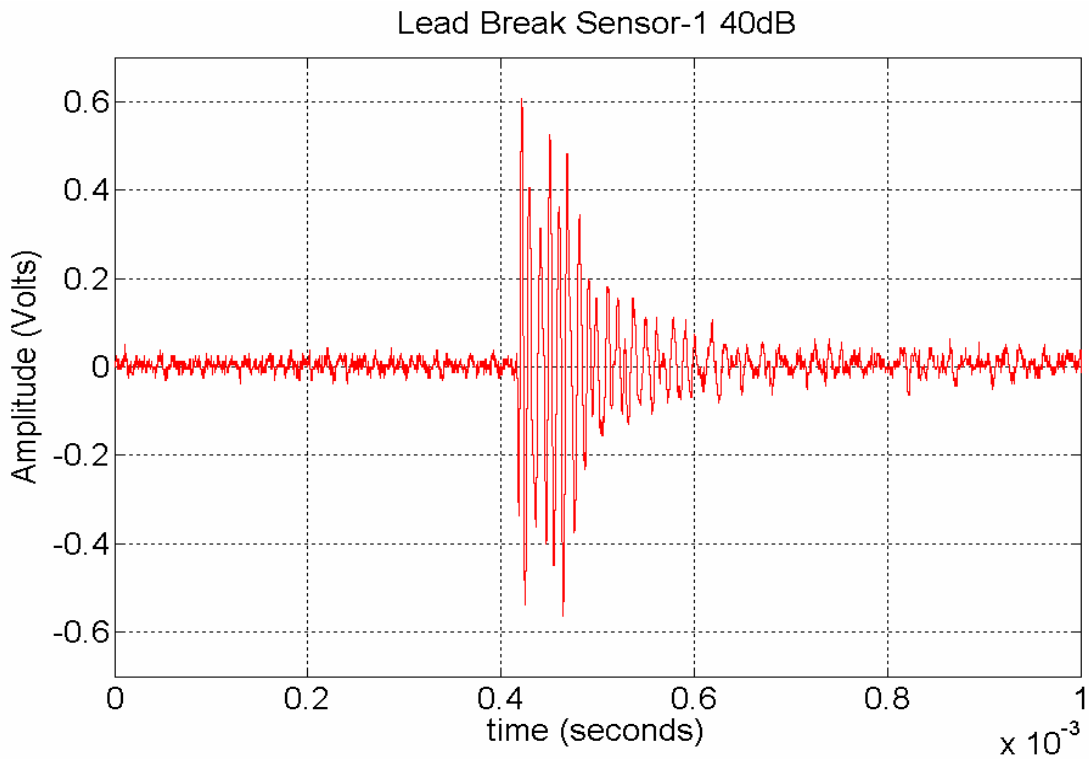


Figure 6.7 Lead break response for sensor-1
Lead Break Sensor-2 40dB

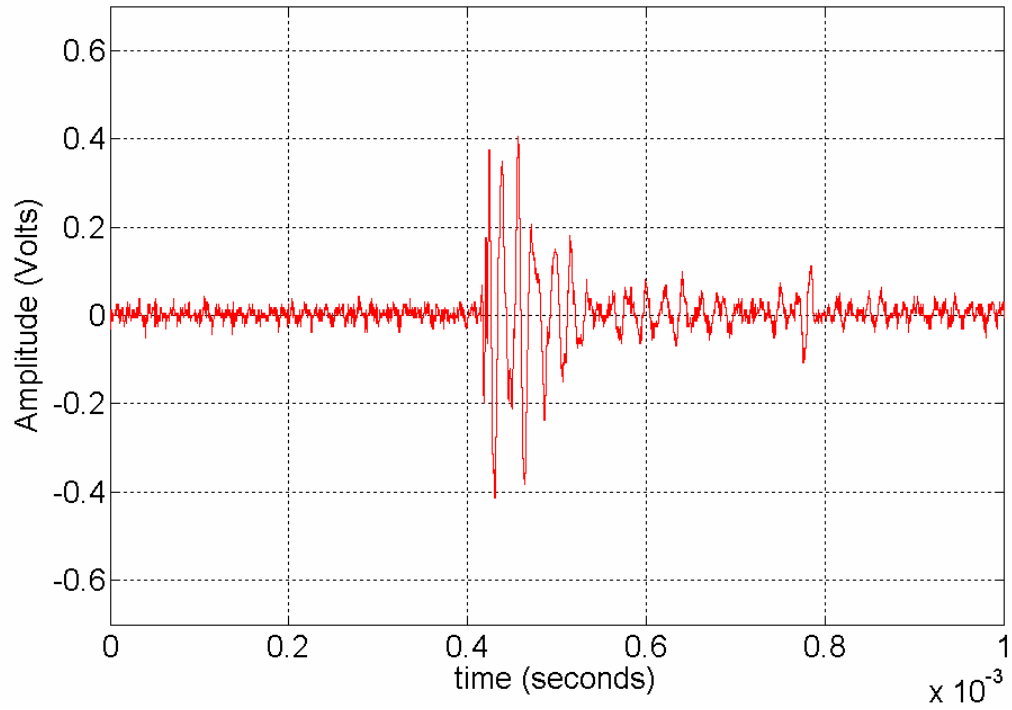


Figure 6.8 Lead break response for sensor-2

Lead Break Sensor-3 40dB

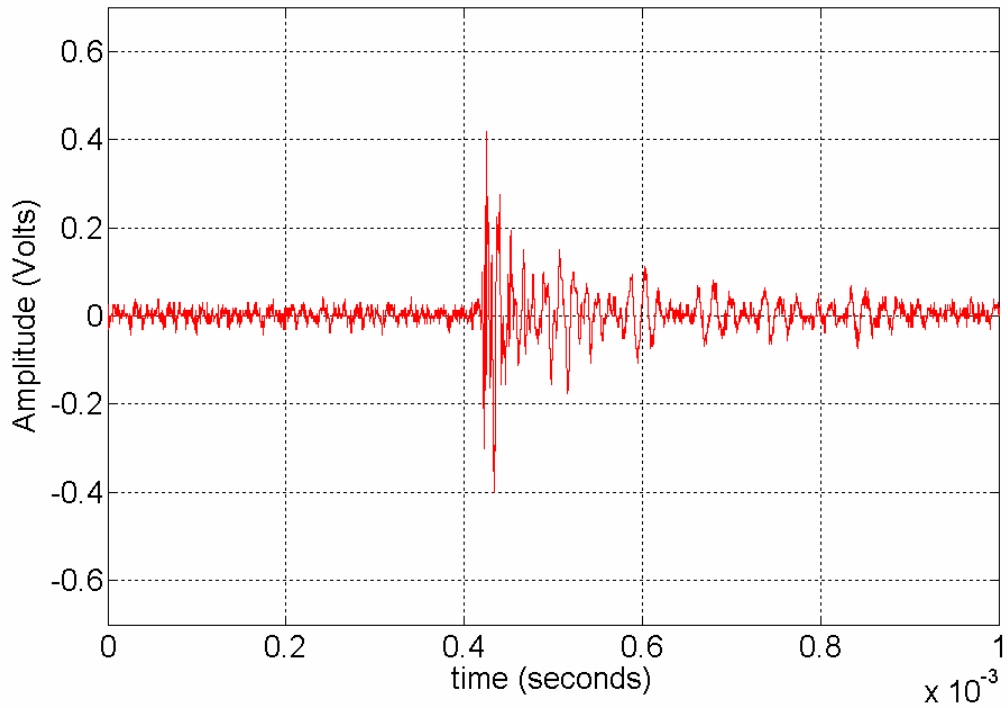


Figure 6.9 Lead break response for sensor-3

For Figures 6.7, 6.8 and 6.9 it can be seen that the sensors do pickup high frequency.

Figures 6.10(a) shows the response of sensor 2 only while Figure 6.10(b) shows the Fast Fourier transform of the acquired data i.e. the frequency information for sensor-2

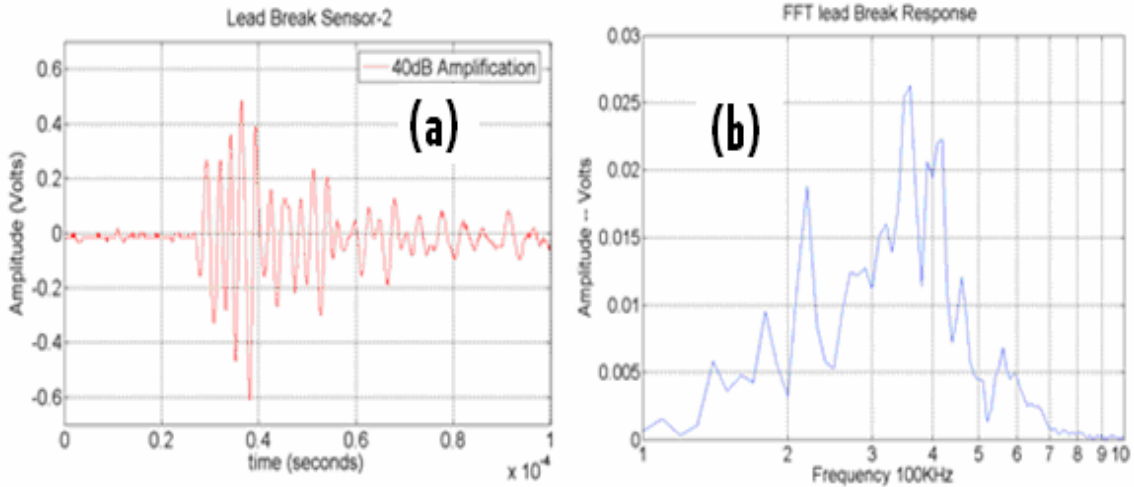


Figure 6.10 Lead break response for sensor-2 (a) and frequency response for sensor-2 (b)

It can be seen from Figure 6.10 (b) that the AFC sensor does pick up high frequency A.E. waves generated due to the lead break with most of the energy concentrated near 300 KHz. The AFC sensor does detect AE emission which can be seen from Figures 6.7, 6.8, 6.9. However the SNR to noise ratio is poor. Once the signal is filtered it shows the clear acoustic emission signal. The raw signal from the sensor needs to be preamplified and filtered which is done by using a commercial filter manufactured by Kron-Hite. In further development of the sensor, an in house preamplifier and filter will be built to replace the commercial filter.

6.3 High frequency response of the sensors in a series connection (Lead Break)

The three sensors on the plate were connected in series. The response was filtered using a bandwidth Kron-Hite filter in a range of 30 KHz-500 KHz with a gain of 40dB

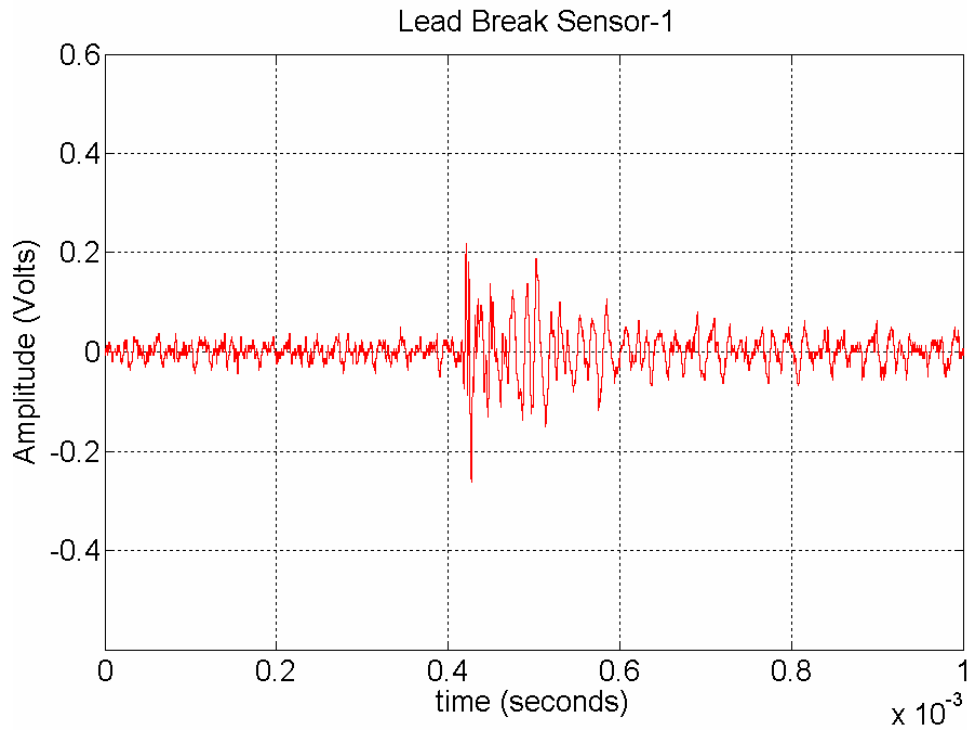


Figure 6.11 Response for Sensors in Series, lead break location near sensor-1

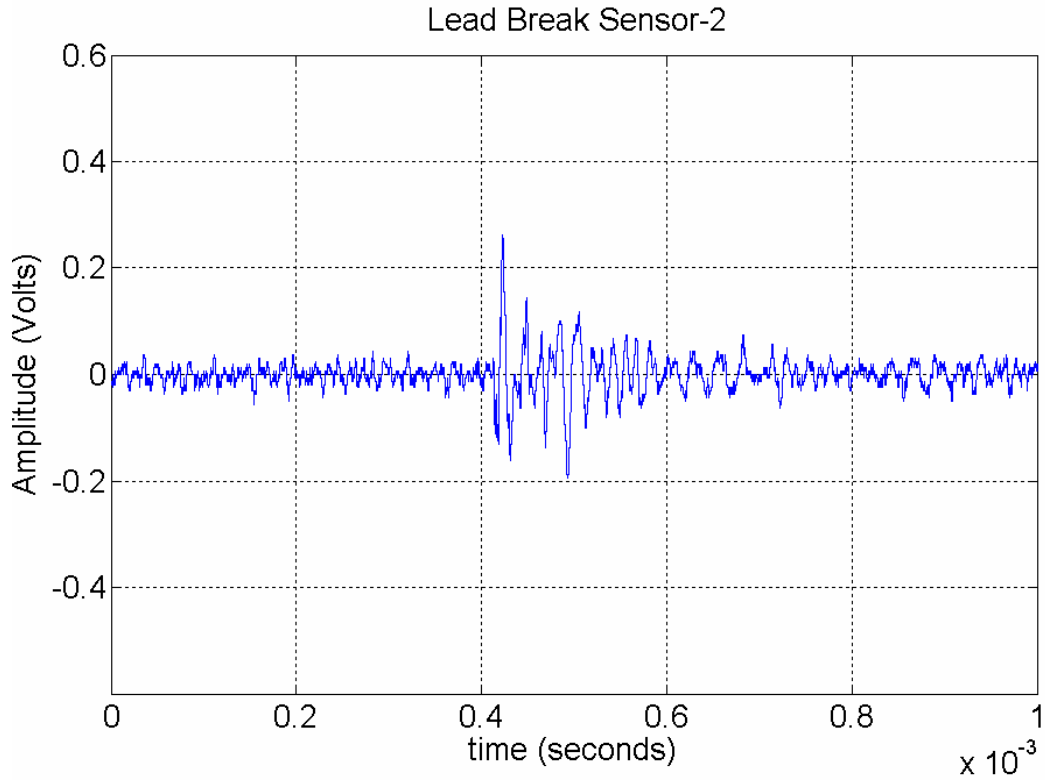


Figure 6.12 Response for Sensors in Series, lead break location near sensor-2

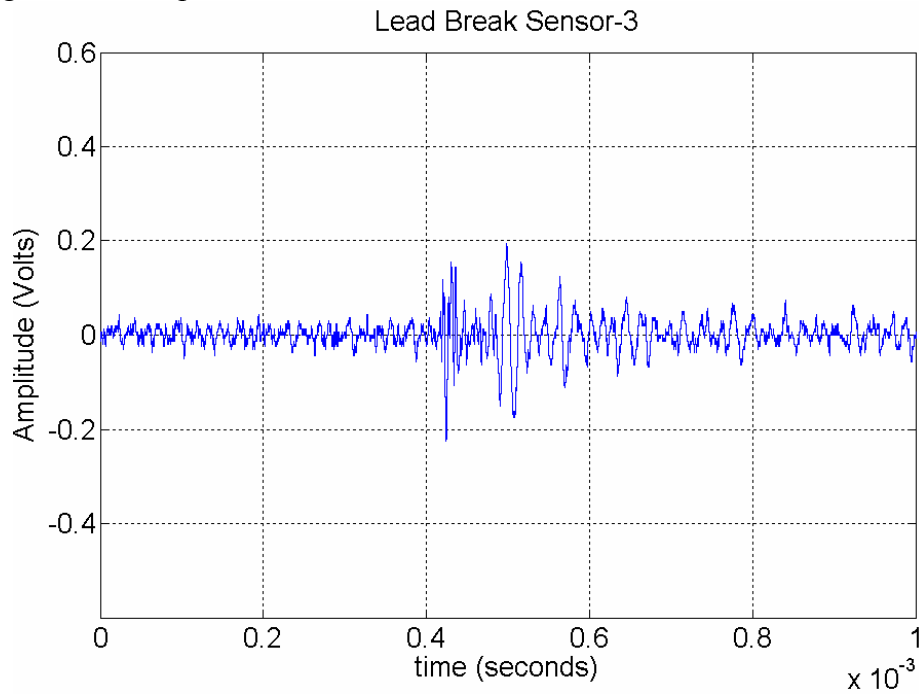


Figure 6.13 Response for Sensors in Series, lead break location near sensor-3

Figures 6.11, 6.12, 6.13 shows that the sensors do pickup simulated AE emission when connected in series.

6.4 High frequency response of the sensors for a parallel connection (Lead Break)

The sensors are connected in parallel and the data was acquired using the Kron-hite filer, with a gain of 40dB. The response is acquired for three different lead break locations the responses are shown in figures 6.14, 6.15, 6.16.

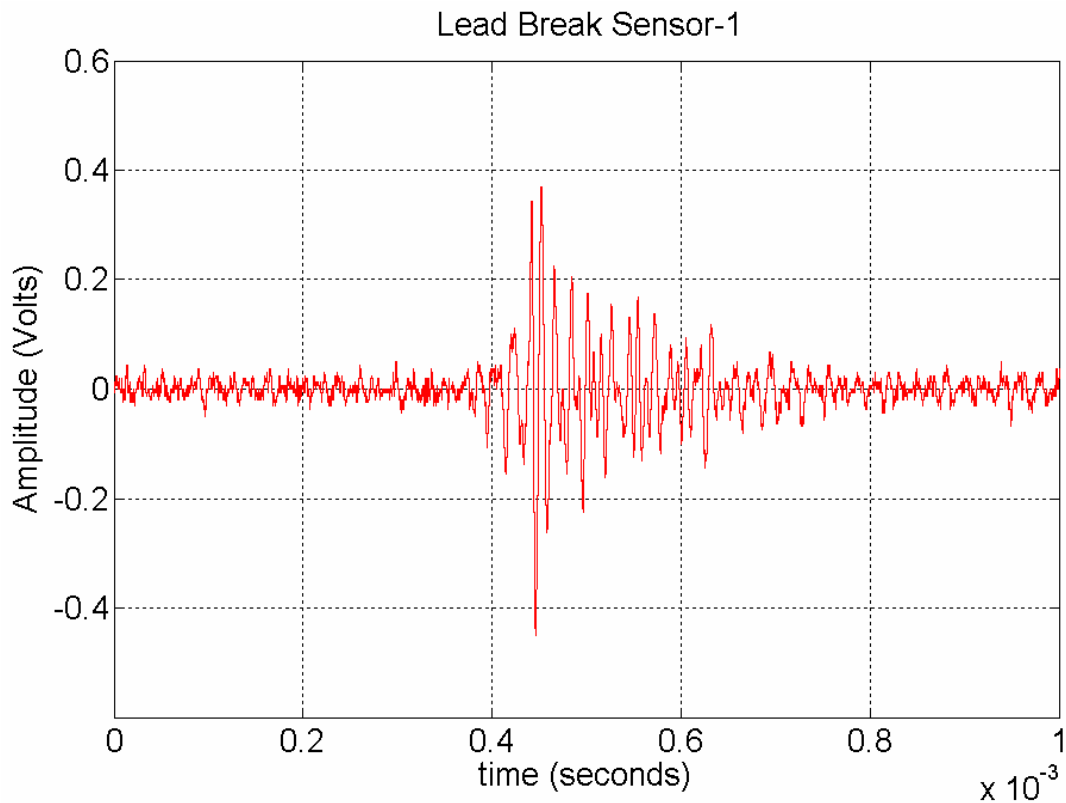


Figure 6.14 Response for Sensors in parallel, lead break location near sensor-1

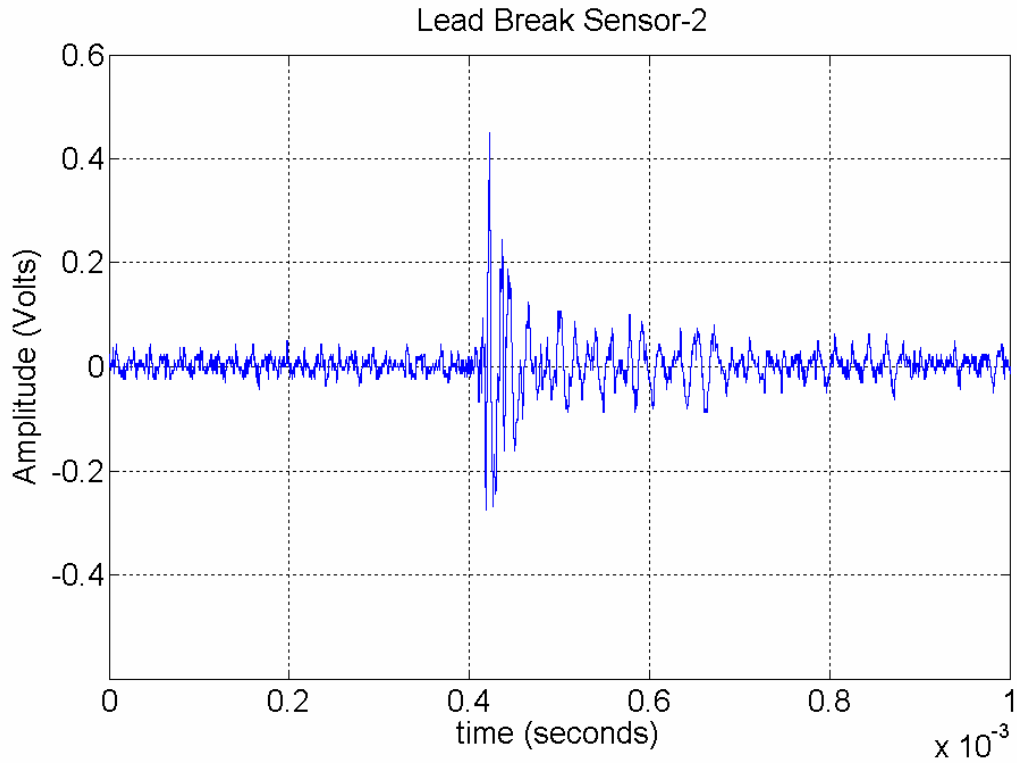


Figure 6.15 Response for Sensors in parallel, lead break location near sensor-2

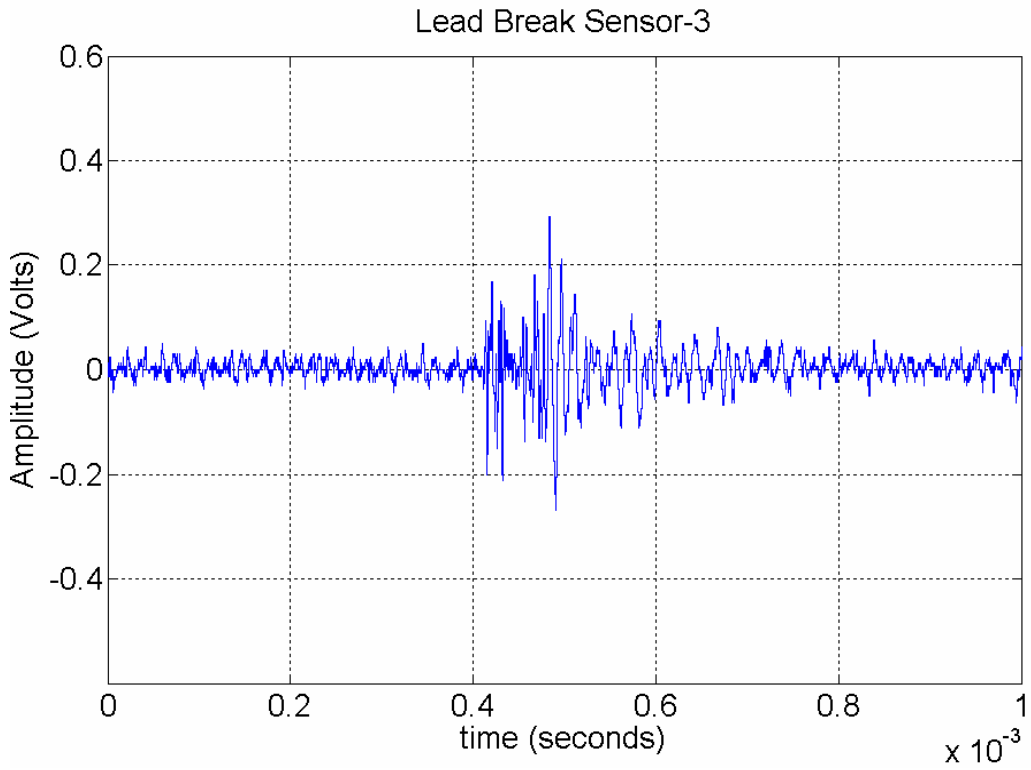


Figure 6.16 Response for Sensors in parallel, lead break location near sensor-3

The Figures 6.14, 6.15 and 6.16 show that the sensors do pickup AE waves when connected in parallel. An attempt has been made to connect the sensors in series and parallel fashion to form the continuous sensor. Table 6.2 gives the comparison of the responses for lead break results for an individual sensor, sensors connected in parallel and series

Table 6.2 Comparison of Results

Parameter	Individual	Parallel	Series
Peak Voltage	0.4V	0.39V	0.21V
Capacitance	0.307nF	0.910nF	0.1nF

The results tabulated in Table 6.2 are expected results. The capacitance value in series will always be less than when the sensors are connected in parallel. When the sensors are connected in series or parallel, the only sensor that contributes to the output is the one near which the lead break is done, while the remaining two sensors add as an impedance to the flow of current resulting in drop of the voltage which can be seen in Table 6.2.

6.5 AFC actuation

The sensor-2 is used as an actuator using a sine wave with amplitude of approximately 100V. The response is then measured at other two sensors i.e. at sensor-1 and sensor-3 as shown in Figure 6.17.

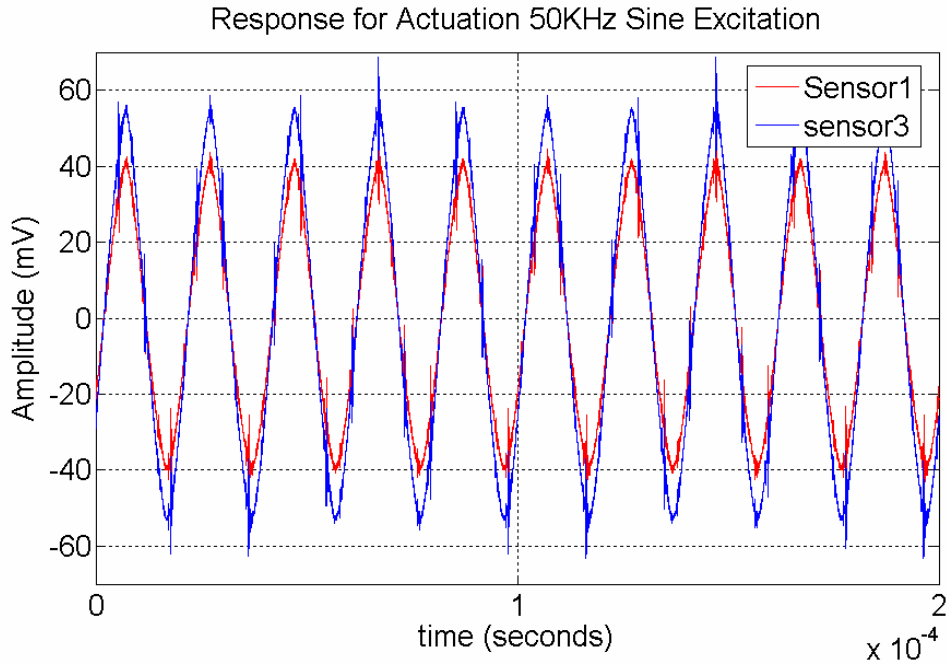


Figure 6.17 Response of Sensors-1 and 3 for actuation at AFC-2

The actuation frequency is varied from 5Hz to 250 KHz and the response is measured at sensor-1 and sensor-3. Figure 6.18 shows the response of the sensor-2 for different actuation frequencies.

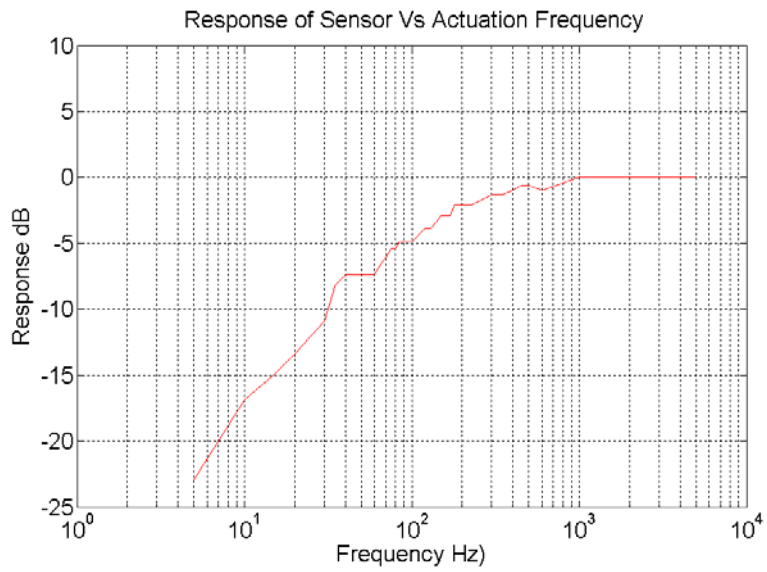


Figure 6.18 Response of Sensors-1 and 3 for actuating sensor-2

The Possible reason for the poor response at lower frequencies can be because of the poor bonding of sensor to the fiber

6.6 Power Harvesting

For power harvesting, a mechanical test machine is used and the voltage signal generated by the AFC sensor is acquired using a 200 MHz Tektronix oscilloscope. Figure 6.19 shows the test setup. The plate is mounted on the MTS machine for a four point bending test. A known sinusoidal loading cycle of 5 Hz is applied to load the beam and response from sensor-2 is observed. The loading sinusoidal cycle is shown in Figure 6.20



Figure 6.19 Experimental setup for power harvesting of sensors bonded on the beam

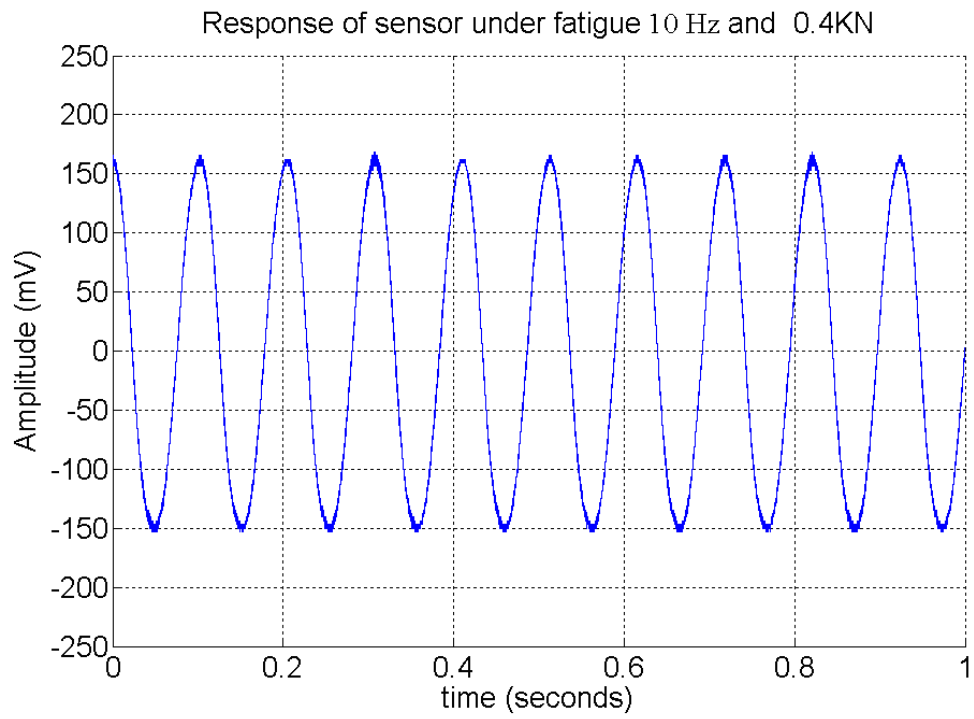


Figure 6.20 Response from sensor-2 under sinusoidal MTS loading

Power calculation is done as follows:

$$P = VI \quad (6.1)$$

where P = peak sinusoidal power generated, V = voltage and I = current, rearranging gives

$$P = \frac{V^2}{R} \quad (6.2)$$

where R is the resistance of the oscilloscope. Substituting $V=0.15V$ and $R=1M\Omega$ in equation (6.2) we get $P = 0.225\mu W$.

6.7 Calculating the d_{31} coefficient

For the beam under fatigue strain occurs in the Z -direction, and the AFC sensor is poled in the Y -direction perpendicular the plane of the beam. The configuration is shown in Figure-6.21.

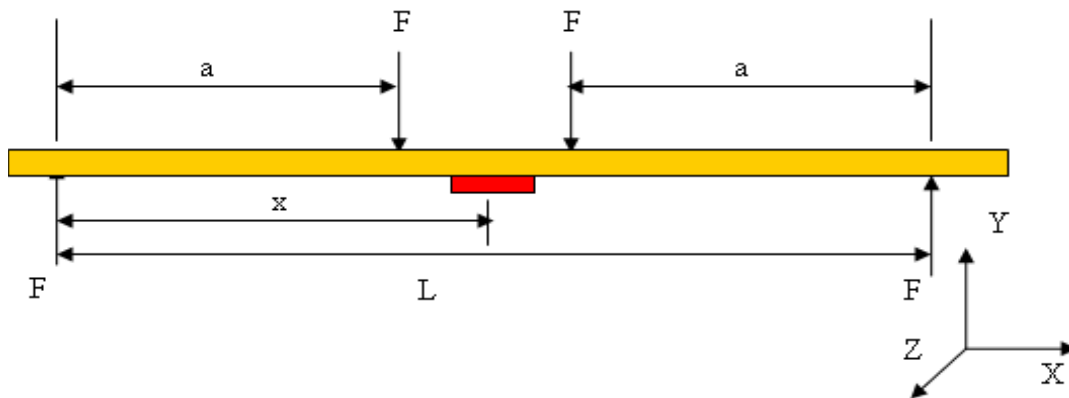


Figure 6.21 A composite beam under loading

Here the direction of the PZT is in the Y -axis of the beam. For the beam under 4 point bending load the deflection is given by

$$\delta_{BC} = \frac{Fa}{6EI} (3x^2 + a^2 - 3Lx) \quad (6.3)$$

Where δ_{BC} = deflection of the beam at a distance 'x'

For $x = \frac{l}{2}$ $\delta_{BC} = \delta_{\max}$, $\delta_{\max} = \frac{Fa}{24EI} (4a^2 - 3L^2)$

$$EI = \frac{Fa}{24\delta_{\max}} (4a^2 - 3L^2) \quad (6.4)$$

where E is the Youngs Modulus and I is the area moment of inertia of the beam

For a beam under bending the stress ' σ ' is given by

$$\sigma = ES_1 = \frac{My}{I} \quad (6.5)$$

Where S_1 = strain in the beam, M= bending moment, y = distance of the fiber from the neutral axis

$$ES_1 = \frac{-My}{I} \quad (6.6)$$

$$S_1 = \frac{-My}{EI} \quad (6.7)$$

Substituting 'EI' in equation of S_1 we get

$$S_1 = \frac{-24\delta_{\max} My}{Fa(4a^2 - 3L^2)} \quad (6.8)$$

From equation (2.1) in Chapter 2

$$V = \frac{e_{31} A S_1}{C_p} + V_0 \quad \text{but} \quad e_{31} = \frac{d_{31}}{s_{11} E} \quad \therefore V = \frac{d_{31} A S_1}{s_{11} E C_p} + V_0 \quad \text{substituting for } S_1 \text{ from equation} \quad (6.8)$$

$$V = \frac{d_{31} A_e}{s_{11} E C_p} \frac{-24\delta_{\max} My}{Fa(4a^2 - 3L^2)} + V_0$$

$$d_{31} = \frac{V_s E_{11}^E C_p F a (4a^2 - 3L^2)}{A_e 24 \delta_{\max} M y} \quad (6.9)$$

Substituting the values from Table 6.1 gives $d_{31} = 80 \times 10^{-12} \frac{C}{N}$. This is about 50% of the expected theoretical value of $80 \times 10^{-12} \frac{C}{N}$. This can be attributed to the fact that the bonding between the sensor and the fiber glass is not perfect resulting in poor strain transformation to the AFC sensor.

Table 6.1 Values used in equation 6.9.

Parameter	Value
V	0.15 volts
s_{11}^E	$1.88 \times 10^{-12} \frac{m^2}{N}$
C_p	0.33nF
F	150N
a	0.09m
L	0.254m
A_e	$4.5e-006 m^2$
δ_{\max}	1.6e-006 m
M	12.858N-m
y	0.000013m

The calculated electromechanical coefficient or d_{31} is expected to be less than the theoretical one because of loss in strain transformation due to bonding layer and Kapton[®] sheets used and the narrow width of the sensor which is probably more sensitive to shear lag. A way to investigate this is to bond the AFC sensor directly on the fiber glass plate without the Kapton[®] sheet using the silver conductive epoxy as shown in Figure-3.6 and measuring the response and compare it with the existing results.

Chapter 7 Conclusion

A data acquisition system and sensors for a technique of structural health monitoring based on a structural neural system and continuous sensors was developed. Testing on an aluminum beam indicated that the SNS analog processor using conventional monolithic piezoceramic sensors was able to detect the acoustic emissions. The acoustic emission level in aluminum was small but detectable. A higher sensitivity of the neural system is needed. An AFC sensor was manufactured in the Smart Structure and BioNanotechnology laboratory [4] with fibers from CeraNova Corporation. These were tested for low frequency tapping, high frequency AE and for power harvesting. The laboratory testing has shown that the AFC sensor manufactured in house can detect and locate simulated acoustic emissions generated on composite panels. Extending this architecture to handle a large number of sensors would make the SNS capable of reducing the number of data acquisition channels typically required by a factor of 10 or more. Connecting the sensor in series forms the continuous sensor which allows many sensor nodes to be connected together to tremendously reduce the number of channels of data acquisition needed to detect acoustic emissions. A standard sensor fabrication method is being developed to produce continuous sensors

Chapter 8 Future Work

Although this system is working successfully, there is still room for further work:

8.1 Data acquisition system

The DAQ system developed needs improvement which are mentioned below:

- Developing a control system using LabVIEW for controlling the MTS controller
- Real-time integration of offline analysis like smoothing of the data, plotting of the sensors firing against time
- Eliminating the use of Matlab[®]
- Currently the user interface elements are rudimentary. To increase productivity, it might be desirable to add features to make them more user friendly and advanced (such as better table editing features)
- Although algorithmic state machines (a programming paradigm) are used for the main control routine, it might be beneficial to extend this concept to some of the other routines, such as the file management VI. Most important for the shm.vi system will be better algorithms which will take less time for acquiring, analyzing and presenting data.
- Currently the rate of crack growth is measured using Vernier Calipers; the accuracy can be improved by using equipments like a camera interfaced to the computer which takes pictures at every acoustic emission

8.2 Active Fiber Sensor

The AFC manufactured have a room for improvements. These are:

- Sensor thickness: As explained in section 3.2 the ideal thickness for sensor is equal to the thickness of the fiber. Currently the sensor thickness is more than that. The thickness can be reduced by machining the mold around the edges.
- Sensor length: The current design of the mold allows a maximum length of 4 inches. The mold needs to be redesigned to manufacture longer length sensors
- Sensor electroding: Using sputtering instead of silver conductive epoxy for placing the electrodes on the AFC preform

References

- [1] **Design of a Wireless Active Sensing Unit for Structural Health Monitoring**, Jerome P. Lynch et.al, Department of Civil and Environmental Engineering, Stanford University, Stanford, CA, 2002.

- [2] **Fiber optic sensor array for multi-dimensional strain measurement**, Barry G Grossmann and Li-Tien Huang Florida Institute of Technology, Electrical Engineering Program, 150 West University Boulevard, Melbourne, FL 32901-6988, USA

- [3] **Health monitoring of aerospace structures with acoustic emission and acousto-ultrasoncs**, RD Finlayson, M Friesel, M Carlos and J C Lenain based on a paper presented at 15th World Conference on NDT, Rome, and October 2000

- [4] **Smart Structures and Bio-Nano Laboratory**, Department of Mechanical Engineering, University of Cincinnati OH-45221-0072

- [5] Fiber optic sensor array for multi-dimensional strain measurement **Barry G Grossmann and Li-Tien Huang** Florida Institute of Technology, Electrical Engineering Program, 150 West University Boulevard, Melbourne, FL 32901-6988, USA

- [6] **Design of a Wireless Active Sensing Unit for Structural Health Monitoring**, Jerome P. Lynch et.al., Department of Civil and Environmental Engineering, Stanford University, Stanford, CA, 2002.
- [7] Bent, A. A “Active **Fiber Composites for Structural Actuation**”, Thesis submitted to Department of Aeronautics and Astronautics at Massachusetts Institute of Technology, 1997, ASML # 97-1.
- [8] **An artificial neural system with distributed parallel processing for structural health monitoring [electronic resource] / Goutham R. Kirikera**
Thesis submitted to the faculty of the University of Cincinnati Ohio 2003
- [9] Goutham R. Kirikera, Saurabh Datta, SriLaxmi Pammi, Courtney Brown, Mark J. Schulz, Mannur J. Sundaresan, “**Recent Advances in an Artificial Neural System for Structural Health Monitoring**,” abstract submitted, SPIE 10th International Symposium, NDE for Health Monitoring and Diagnostics, San Diego, CA, March 2-6, 2003.
- [10] Saurabh Datta, Goutham R. Kirikera, Mark J. Schulz, Mannur J. Sundaresan, “**Sensor Design for An Artificial Neural System**,” Ninth International Conference on Composites Engineering, July 1-6, 2002, San Diego, CA.
- [11] Schulz, M.J., Chattopadhyay, S., Sunderesan, M.J., Ghoshal, A., Martin, W.N., Pratap, P.R., “**Processing , Understanding and applications of Piezoceramic Materials for an Artificial Neural System.**” Ceramic Materials Symposium at the international Mechanical Engineering Congress and Exposition Winter

Annual Meeting of the ASME, Nov.11-16, 2001, New York Hilton and Towers, NY.

- [12] Sundaresan, M.J., Schulz, M.J., Ghoshal, A., Pratap, P., "**A Neural System for Structural Health Monitoring**," SPIE 8th International Symposium on Smart Materials and Structures, March 4-8, 2001.
- [13] **Electrical Properties of Macro-Fiber Composite Actuators and Sensors**, Justin Michael Lloyd, Thesis submitted to the faculty of the Virginia Polytechnic Institute and State University, VA June 2004
- [14] [.http://www.ceramtec.de/intl/e4/ta=e4*247/la=en/ta0=gb*108/ta1=e3*421/le=2/](http://www.ceramtec.de/intl/e4/ta=e4*247/la=en/ta0=gb*108/ta1=e3*421/le=2/)
- [15] Hagood, N.W., Kindel,R., Ghandi, K., and Gaundenzi,P., 1993, "**Improving Transverse Actuation of Piezoceramics using Interdigitated Surface Electrodes**", SPIE Paper No. 1917-25, Proceedings of 1993 North American Conference on Smart Structures and Materials, Albuquerque, NM.
- [16] Eric H. Anderson, Mark D. Holcomb, Donald J. Leo CSA Engineering, Inc. Mountain View, CA "**Integrated Electromechanical Devices for Active Control of Vibration and Sound**" Adam X. Bogue, Farla R. Russo Active Control eXperts, Inc. Cambridge MA.
- [17] **Center Macro-Fiber CompositeActuator (LaRC-MFC): Technical Overview NASA-Langley Research** W. Keats Wilkie Robert G. Bryant, James W. High, Robert L. Fox, Bruce D. Little,Paul H. Mirick, Richard F. Hellbaum, Anthony Jalink

- [18] **Active fiber composite continuous sensors for structural health monitoring**, Saurabh Datta Thesis Submitted to University of Cincinnati Ohio 2003
- [19] Saurabh Datta, Goutham R. Kirikera, SriLaxmi Pammi, Courtney Brown, Mark J. Schulz, Mannur J. Sundaresan, “**Continuous Sensors for Structural Health Monitoring**,” abstract submitted, SPIE 10th International Symposium, NDE for Health Monitoring and Diagnostics, San Diego, CA, March 2-6, 2003.
- [20] Datta, S., Kirikera, G.R., Sundaresan, M.J., Schulz, M.J., “**Active Fiber Composite Continuous Sensors**,” International conference on Smart Materials, Structures and System (ISSS-SPIE 2002), December 12-14, 2002, Bangalore India.
- [21] Sunderesan, M.J., Ghoshal A., Martin, W.N. and Schulz, M.J. “*A continuous Sensor to measure Acoustic Waves in Plates*” Journal of Intelligent Material Systems and Structures, vol.12, No.1 pp.41-57, January 2001.
- [22] **CeraNova Corporation**, 101 Constitution Boulevard, Suite D, Franklin, MA 02038-2587.
- [23] **Smart Structures Analysis and Design**, A.V. Srinivasan, D Michael McFarland.
- [24] **Structural Health Monitoring of Composite Materials Using Piezoelectric Sensors**, Seth S. Kessler and S. Mark Spearing.

- [25] Saurabh Datta, Goutham R. Kirikera, SriLaxmi Pammi, Courtney Brown, Mark J. Schulz, Mannur J. Sundaresan, “**Continuous Sensors for Structural Health Monitoring**,” abstract submitted, SPIE 10th International Symposium, NDE for Health Monitoring and Diagnostics, San Diego, CA, March 2-6, 2003.
- [26] Goutham R. Kirikera, Saurabh Datta, Mark J. Schulz, Mannur J. Sundaresan, “**An Artificial Neural System for Health Monitoring of Large Structures**,” Ninth International Conference on Composites Engineering, July 1-6, 2002, San Diego, CA.
- [27] Pedemonte, P. et.al., “**Signal Processing for Passive Impact Damage Detection in Composite Structures**”, Smart Structures and Materials 2001 : Modeling, Signal Processing and Control in Smart Structures, Proceedings of SPIE vol. 4326, 2001.
- [28] Schulz, M.J., Sundaresan, M.J., McMichael, M., Clayton, D., “**Evaluation of Piezoceraic Materials at Moderately Elevated Temperatures**”, Proceedings of IMECE’02, 2002 ASME International Mechanical Engineering Congress & Exposition, New Orleans, Louisiana, November 17-22,2002.
- [29] Muralt, P., “**PZT Thin Films for Microsensors and Actuators: Where Do We Stand?**”, IEEE Transactions on Ultrasonics, Ferroelectrics and Frequency Control, vol.47, no.4, pp.903-915, July 2000.

- [30] Giurgiutiu, V., Chaudry, Z., C.A. Rogers, 1995, “**Energy –Based Comparison of Solid-State Actuators**”, Centre for Intelligent Material Systems and Structures, Report no. CIMSS 95-101.
- [31] Wang, C.S. and Chang, F.K., “**Built in Diagnostics for Impact Damage Identification of Composite Structures**”, Proceedings of the 2nd International Workshop on Structural Health Monitoring, pp. 612-621, San Francisco, CA, 1999.
- [32] Keilers, C and Chang, F.K. “**Damage Detection and Diagnostics for Composite Structures Using Built-in Piezoceramics**”, Proceedings of SPIE, vol. 1917, pp. 1009-1019, San Diego, CA, 1993.
- [33] Fu-Kuo Chang “**Structural Health Monitoring The Demands and Challenges**” Proceedings of the 3rd International workshop on structural health monitoring, Stanford, CA. Sep-12-14, 2001.
- [34] Taylor et al. “ **Piezoelectricity Ferro electricity and related phenomena**” vol.4. Gordon and Breach 1985.
- [35] Cady W.G., “**Piezoelectricity: an introduction to the theory and applications of electromechanical phenomenon in crystals.**” (Dover, NY, 1964).
- [36] “**A Software Framework For Neuroscience Experiments Involving Auditory and Visual Stimuli**”, Virantha N. Ekanayake Bachelor of Engineering Project Report/ Honors Thesis, Thayer School of Engineering Dartmouth College Hanover, New Hampshire, June 8, 1999.

- [37] **“Structural Health Monitoring Static Test of a Wind Turbine Blade”**, M.J. Sundaresan, M.J. Schulz, and A. Ghoshal Intelligent Structures and Mechanisms (ISM) Laboratory, Department of Mechanical Engineering North Carolina A&T State University Greensboro, North Carolina subcontract report August 1999, March 2002 • NREL/SR-500-28719.
- [38] **“Design and performance of a self-sensing, self-actuating piezoelectric monomorph with interdigitated electrodes”**, Yong K. Honga, Heung-Keun Parka, Sung Q Leeb, Kee S. Moon, Raghav R. Vangac, and M. Levyc, Proceedings of the SPIE International Conference on Opto-mechatronic Actuators, Sensors and Control, SPIE, Philadelphia, Vol. 5602, pp. 210-217, October 2004.
- [39] **“Characterization of Piezoelectric Wafer Active Sensors”**, Victor Giurgiutiu and Andrei N. Zagrai, University of South Carolina, Department of Mechanical Engineering, Columbia, SC 29208, Journal Of Intelligent Materials Systems And Structures, Vol. 11 – December 2000.
- [40] **“Damage Detection In Simulates Aging-Aircraft Panels Using The Electro-Mechanical Impedance Technique”**, Victor Giurgiutiu and Andrei Zagrai, Department of Mechanical Engineering University of South Carolina, Columbia, SC 29208, Adaptive Structures and Material Systems Symposium, ASME Winter Annual Meeting, Nov. 5-10, 2000, Orlando, FL.

- [41] **“Demonstration and characterization of PZT thin-film sensors and actuators for meso- and micro-structures”**, Yi-Chu Hsua, Chia-Che Wu b, Cheng-Chun Lee b, G.Z. Caoc, I.Y. Shen b, 2004 www.sciencedirect.com.
- [42] **“Implementation of Advanced Fiber Optic and Piezoelectric Sensors Fabrication and Laboratory Testing of Piezoelectric Ceramic-Polymer Composite Sensors for Weigh-in-Motion Systems”**, Dr. Ali Maher, Mr. Patrick J. Szary, Dr. Ahmad Safari, Dr. Raj K. Panda, Final report submitted to NJDOT February 1999 FHWA NJ 1999-029.
- [43] **“Design, Fabrication and Experimental-Numerical Study of PZT Sensors”**, M. Arik, S. M. Zurnx, K. S. Yigit, and A. Bar-Cohen, Laboratory for Thermal Management of Electronics, Department of Mechanical Engineering, Microtechnology Laboratory, Department of Electrical Engineering, University of Minnesota, Minneapolis, MN 55455.
- [44] **“Electrical Properties And Power Considerations Of A Piezoelectric Aactuator, T. Jordan, Z. Ounaies, J. Tripp, and P. Tcheng”**, NASA-Langley Research Center, Hampton, VA 23681, ICASE, NASA-Langley Research Center, Hampton, VA 23681, USA.
- [45] **“The influence of temperature and bonding thickness on the actuation of a cantilever beam by PZT patches”**, Cu-Hai Nguyen, Stanislaw Pietrzko and Rudolf Buetikofer, 16 June 2004, Online at stacks.iop.org/SMS/13/851 doi:10.1088/0964-1726/13/4/023.

- [46] **“Experiments And Technologies For Decentralized Temperature Control”**, Nicanor Quijano, Thesis Degree Master of Science in the Graduate School of The Ohio State University, 2002.
- [47] **“The use of 0-3 piezocomposite embedded Lamb wave sensors for detection of damage in advanced fibre composites”**, R A Badcock and E A Birt, Structural Materials Centre, DERA Farnborough, Hampshire GU14 0LX, UK, Smart Mater. Struct. 9 (2000) 291–297. Printed in the UK, PII: S0964-1726(00)13239-2.
- [48] **“Computational Material Characterization of Active Fiber Composite”**, Tae Ho Yoon, Seung Hoon Paik, Sang Joon Shin, Seung Jo Kim, Department of Aerospace Engineering Seoul National University Korea.
- [49] **"LabVIEW - Graphical Programming for Instruments, User Manual"**, National Instruments, 1996.
- [50] L.K. Wells, **"LabVIEW Student Edition User's Guide"**, National Instruments, 1995.
- [51] **"Data Acquisition Basics Manual"**, National Instruments, 11500 N Mopac Expwy Austin, TX 78759-3504 1996.
- [52] **“A Structural Neural System”** Goutham R.Kirikera, Inpil Kang, Vishal Shinde, et.al Smart Structures and Materials 2005 : Proceedings of SPIE.

Appendix A

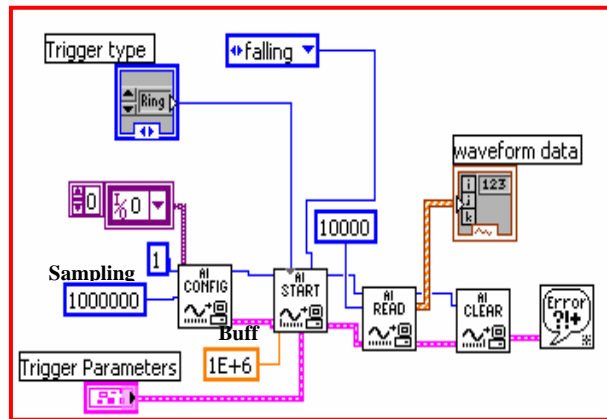
LabVIEW Code Description

A brief summary on the actual LabVIEW code structure is given here. Please note that no attempt will be made to go into any great detail on the actual operation of each routine as these are documented within the source code diagrams. In addition source code diagrams are difficult to include in hard copy format because of their structure – for instance case structures have several overlapping sections of code, of which only one is visible at any one time on the screen. Including printouts of these would be quite useless as far as comprehending the data goes. Instead, the files are supplied on a disk for viewing on screen.

When data acquisition is performed, the software needs to know the following information:

- Device number
- Channel that is being used
- Sampling Rate
- Trigger type
- Buffer size

This is done by the following part of the VI in Figure A-1



8.2.1.1 Figure A-1 Data acquisition

Stream from Disk

This is done by the following part of the VI

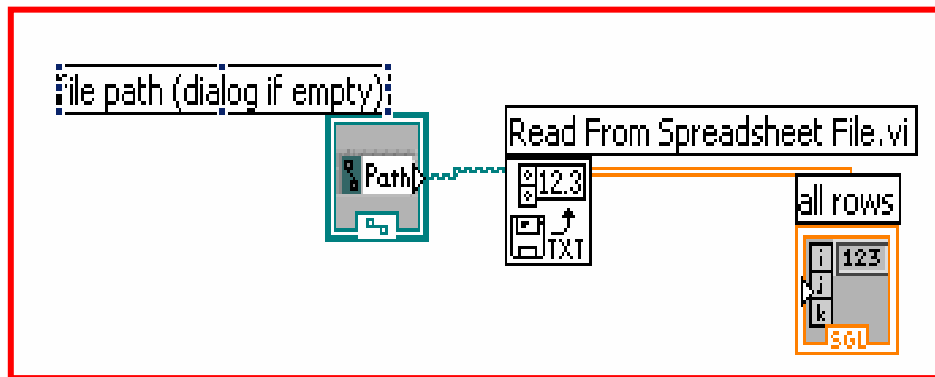


Figure A-2 Stream From Disk

Generate Time and Frequency Data

This is done by the following part of the VI

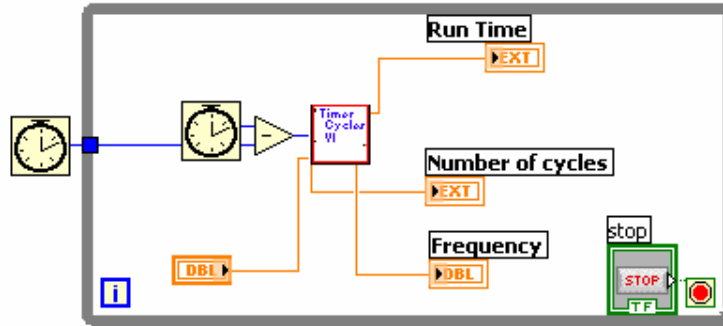


Figure A-3 Generate Time and Frequency Data

Graphical Data Presentation

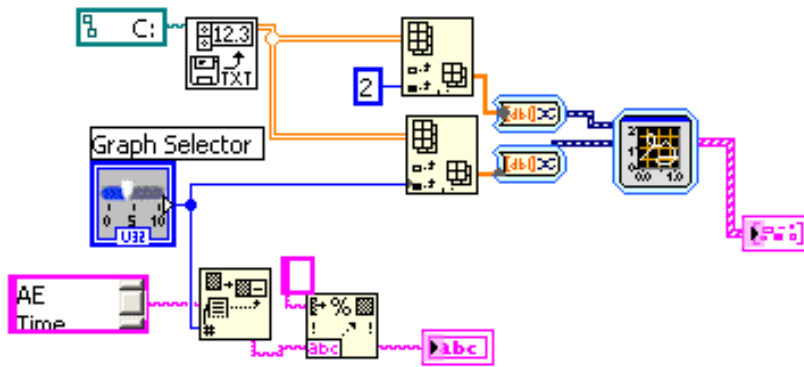


Figure A-4 Graphical Data Presentation

Streaming to Disk

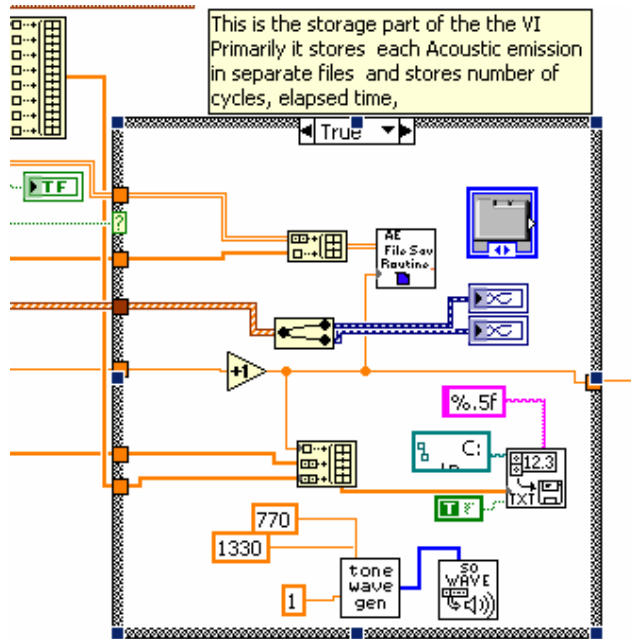


Figure A-5 Stream to Disk

Appendix B

Matlab[®] Script

This script is included in the LabVIEW GUI. It calculates the number of AE hits from the crack information signal and the cumulative Peak amplitude of the time information signal

```
counter1=0;
counter2=0;
counter3=0;
temp=zeros(1,100);
sum=0;
kk=0;
jj=0;
if (length(X)==samples)
Z=abs(X);
for n=1:samples-1
%%%%% conditions to calculate the cumulative voltages
    if((Z(2,n)>threshold) )
        jj=jj+1;
        temp(jj)=Z(2,n);
    end
    if(Z(2,n)>=threshold & Z(2,n+1)<threshold)
        kk=kk+1;
        sum=max(temp)+sum;
        temp=zeros(1,100);
        jj=0;
    end
    %%%%%% conditions to calculate the cumulative no of hits
    if ( X(2,n)>=threshold1 & X(2,n+1)<threshold1)
        counter1 =counter1+1;
    end
    if ( X(2,n)>=threshold2 & X(2,n+1)<threshold2)
        counter2 =counter2+1;
    end
    if ( X(2,n)>=threshold3 & X(2,n+1)<threshold3 )
        counter3 =counter3+1;
    end
end
end
highest=counter1;
medium=counter2-counter1;
```

```
lowest=counter3-counter2;
```

Appendix C

PCI 6110E Board Specifications

This appendix lists the specifications of 6110 E board. These specifications are typical at 25° Celsius unless otherwise noted.

Analog Input Input Characteristics

Number of channels	
PCI-6110E	4 differential
PCI-6111E	2 differential
Resolution.....	12 bits, 1 in 4,096
Max sampling rate	5 MS/s
Min sampling rate	1 kS/s
Analog input characteristics	
Input coupling	DC/AC
Max working voltage for all analog input channels	
+ input	Should remain within ± 11 V for ranges $\geq \pm 10$ V; should remain within ± 42 V for ranges $< \pm 10$ V
- input	Should remain within ± 11 V
Overvoltage protection	± 42 V
Inputs protected	
+ input	all channels
- input	all channels
FIFO buffer size	8,192 samples
Data transfers	DMA, interrupts, programmed I/O
DMA modes.....	Scatter-gather

Transfer Characteristics

INL	± 0.5 LSB typ, ± 1 LSB max
DNL.....	± 0.3 LSB typ, ± 0.75 LSB max
Spurious free dynamic range (SFDR). See table, analog input characteristics	
Effective number of bits (ENOB).....	11.0 bits, DC to 100 kHz
Offset error	See table, analog input characteristics

Amplifier Characteristics

Input impedance	1 M Ω in parallel with 100 pF
Input bias current	± 200 pA
Input offset current.....	± 100 pA
CMRR.....	See table, analog input characteristics

Dynamic Characteristics

Interchannel skew	1 ns typ
$f_{in} = 100$ kHz	
input range = ± 10 V	
Bandwidth (0.5 to -3 dB)	
Input range $> \pm 0.2$ V	5 MHz
Input range = ± 0.2 V	4 MHz
System noise	See table, analog input characteristics
Crosstalk	-80 dB, DC to 100 kHz

Stability

Recommended warm-up time	15 min.
Offset temperature coefficient	
Pregain	± 5 $\mu\text{V}/^\circ\text{C}$
Appendix A Specifications	
© National Instruments Corporation A-5 PCI-6110E/6111E User Manual	
Postgain	± 50 $\mu\text{V}/^\circ\text{C}$
Gain temperature coefficient.....	± 20 ppm/ $^\circ\text{C}$
Onboard calibration reference	
Level	5.000 V (± 2.5 mV) (actual value stored in EEPROM)
Temperature coefficient	± 0.6 ppm/ $^\circ\text{C}$ max
Long-term stability.....	± 6 ppm/

Analog Output

Output Characteristics

Number of channels	2 voltage
Resolution.....	16 bits, 1 in 65,536
Max update rate	
1 channel	4 MS/s, system dependent
2 channel	2.5 MS/s, system dependent
FIFO buffer size.....	2,048 samples
Data transfers.....	DMA, interrupts, programmed I/O
DMA modes	Scatter gather

Transfer Characteristics

Relative accuracy (INL)	± 4 LSB typ, ± 8 LSB max
DNL.....	± 2 LSB typ, ± 8 LSB max
Offset error	± 5.0 mV max
Gain error	
(relative to internal reference).....	$\pm 0.1\%$ of output range max

Voltage Output

Ranges	± 10 V
Output coupling	DC
1 000 h ,	
Appendix A Specifications	
PCI-6110E/6111E User Manual A-6 © National Instruments Corporation	
Output impedance	50 Ω $\pm 5\%$

Current drive ± 5 mA min
Output stability Any passive load
Protection Short-circuit to ground
Power-on state 0 V

Dynamic Characteristics

Slew rate 300 V/ μ s
Noise 1 mV_{rms}, DC to 5 MHz
Spurious free dynamic range 75 dB, DC to 10 kHz

Stability

Offset temperature coefficient ± 500 μ V/ $^{\circ}$ C
Gain temperature coefficient
Internal reference ± 50 ppm/ $^{\circ}$ C
External reference ± 25 ppm/ $^{\circ}$ C
Onboard calibration reference
Level 5.000 V (± 2.5 mV) (actual
value stored in EEPROM)
Temperature coefficient ± 0.6 ppm/ $^{\circ}$ C max
Long-term stability ± 6 ppm/

Digital I/O

Number of channels 8 input/output
Compatibility TTL/CMOS
1 000 h ,
Appendix A Specifications
© National Instruments Corporation A-7 PCI-6110E/6111E User Manual
Digital logic levels
Power-on state Input (High-Z)
Data transfers Programmed I/O

Timing I/O

Number of channels 2 up/down counter/timers,
1 frequency scaler
Resolution
Counter/timers 24 bits
Frequency scaler 4 bits
Compatibility TTL/CMOS
Base clocks available
Counter/timers 20 MHz, 100 kHz
Frequency scaler 10 MHz, 100 kHz
Base clock accuracy $\pm 0.01\%$
Max source frequency 20 MHz
Min source pulse duration 10 ns, edge-detect mode
Min gate pulse duration 10 ns, edge-detect mode

Triggers

Analog Trigger

Source
PCI-6110E All analog input channels,
external trigger (PF10/TRIG1)

PCI-6111E..... All analog input channels,
external trigger (PFI0/TRIG1)
Level \pm full-scale, internal;
 ± 10 V, external
Slope Positive or negative
(software selectable)
Resolution 8 bits, 1 in 256
Hysteresis..... Programmable
Bandwidth (-3 dB) 5 MHz internal/external
External input (PFI0/TRIG1)
Impedance 10 k Ω
Coupling..... AC/DC
Protection -0.5 V to ($V_{cc} + 0.5$) V when
conFigured as a digital signal,
 ± 35 V when conFigured as an
analog trigger signal or
disabled, ± 35 V powered off

Digital Trigger

Compatibility TTL
Response Rising or falling edge
Pulse width..... 10 ns min

Appendix A Specifications

© National Instruments Corporation A-9 PCI-6110E/6111E User Manual

Bus Interface

Type Master, slave

Power Requirement

+5 VDC ($\pm 5\%$)

PCI-6110E 2.5 A

PCI-6111E 2.0 A

Power available at I/O connector +4.65 to +5.25 VDC at 1 A

Physical

Dimensions

(not including connectors) 31.2 by 10.6 cm (12.3 by 4.2 in)

I/O connector 68-pin male SCSI-II type

Environment

Operating temperature 0° to 45° C

Storage temperature -20° to 70° C

Relative humidity 5% to 90% noncondensing

© National Instruments Corporation B-1 PCI-6110E/6111E User Manual

This appendix lists the specifications of your 611X E board. These specifications are typical at 25° C unless otherwise noted.

FIFO buffer size 8,192 samples

Data transfers..... DMA, interrupts, programmed I/O

DMA modes..... Scatter-gather

Appendix D

Specification of Silver conductive epoxy

Specification of Silver conductive epoxy used for electroding



DATA SHEET

EPO-TEK. H20E

Electrically Conductive, Silver Epoxy

Rev. IV
10/00

TYPICAL PROPERTIES

(To be used as a guideline only)

NUMBER OF COMPONENTS Two
MIXING RATIO PARTS BY WEIGHT
Part "A" (epoxy resin and silver powder) 1
Part "B" (hardener and silver powder) 1
NOTE: Mix contents of each container (A and B) thoroughly before mixing the two together.

CURE SCHEDULE (minimum)
175°C 45 seconds
150°C 5 minutes
120°C 15 minutes
80°C 90 minutes

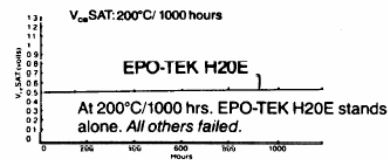
PHYSICAL PROPERTIES
Color Bright Silver
Consistency Smooth, thixotropic paste
Specific Gravity
Part "A" 2.03
Part "B" 3.07
Viscosity (@ 100 rpm/23°C) 2,200 - 3,200 cPs
Glass Transition Temp. (Tg) > 80°C
(cured 150°C/1 hour) typically 100°C
Coefficient of Thermal Expansion (CTE)
Below Tg 31×10^{-6} in/in/°C
Above Tg 120×10^{-6} in/in/°C
Lap Shear Strength 1,500 psi
Die Shear Strength > 10 Kg/ 3,400 psi
Degradation Temperature (TGA) 410°C
Weight Loss @ 200°C 0.16%
Operating Temperature
Continuous 200°C
Storage Modulus 750,000 psi
Volume Resistivity < 0.0004 ohm-cm
Thermal Resistance: (Junction to Case)
TO-18 package with nickel-gold metallized 20 x 20 mil chips and bonded with EPO-TEK H20E (2 mils thick)
EPO-TEK H20E 6.7 to 7.0°C/watt

THERMAL CONDUCTIVITY 29 W/m²K
Based on Thermal Resistance Data: $R = L \times K^{-1} \times A^{-1}$
SCHOTTKY DIODE
INITIAL 2 WEEKS @ 200°C
 C_j 1pF (typical)
 V_f 5V @ 10 µa 4.8V @ 10 µa
 V_f 0.4V @ 1 ma 0.32V @ 1 ma

POT LIFE 4 days
SHELF LIFE
One year when stored at room temperature.
REFRIGERATION NOT REQUIRED

NASA APPROVED
NON TOXIC - complies with USP Class VI
Biocompatibility standards

TO-3 package, 2N3055 chips, medium power transistor-
4 amp pulse



H20E EXHIBITS SUPERIOR V_{ce}SAT PERFORMANCE.

EPO-TEK H20E is a 100% solids, two component silver filled epoxy with a soft, smooth, thixotropic consistency designed specifically for chip bonding in microelectronic and optoelectronic applications. It is also used extensively for thermal management applications due to its high thermal conductivity.

The excellent handling characteristics and the extremely long pot life of this unique Electrically Conductive Adhesive (ECA) are obtained without the use of solvents. In addition to the high electrical conductivity, the short curing cycles, the proven reliability and the convenient mix ratio, EPO-TEK H20E is extremely simple to use and make it an ideal material for use in electronic applications. The pure silver powder is dispersed in both the resin and the hardener so that it can be used in a convenient 1:1 mixing ratio. In fact the EPO-TEK H20E is the easiest-to-use two component silver epoxy that has ever been developed for the microelectronic industry.

EPO-TEK H20E is especially recommended for use in high speed epoxy chip bonding systems where very fast cures are highly desirable. This cannot be obtained with single component systems. Because EPO-TEK H20E can be cured very rapidly, it is an excellent material to use for making fast circuit repairs. EPO-TEK H20E can be screen printed, machine dispensed or stamped and can withstand wire bonding temperatures in the range of 300 - 400°C.

EPO-TEK H20E has proven itself to be extremely reliable over the many years of service and is still the conductive adhesive of choice for new applications.

When placing an order, please specify whether EPO-TEK H20E is to be used by volume or weight.

EPOXY TECHNOLOGY, INC. 14 Fortune Drive Billerica, MA 01821-3972 USA

PHONE: 978.667.3805 1.800.227.2201 FAX: 978.663.9782

This information is based on data and tests believed to be accurate. Epoxy Technology, Inc. makes no warranties (expressed or implied) as to its accuracy and assumes no liability in connection with the use or inability to use this product.